Advanced topics in PFM and SPM of ferroelectrics: surface chemistry effects and imaging in vacuum

Sergei V. Kalinin

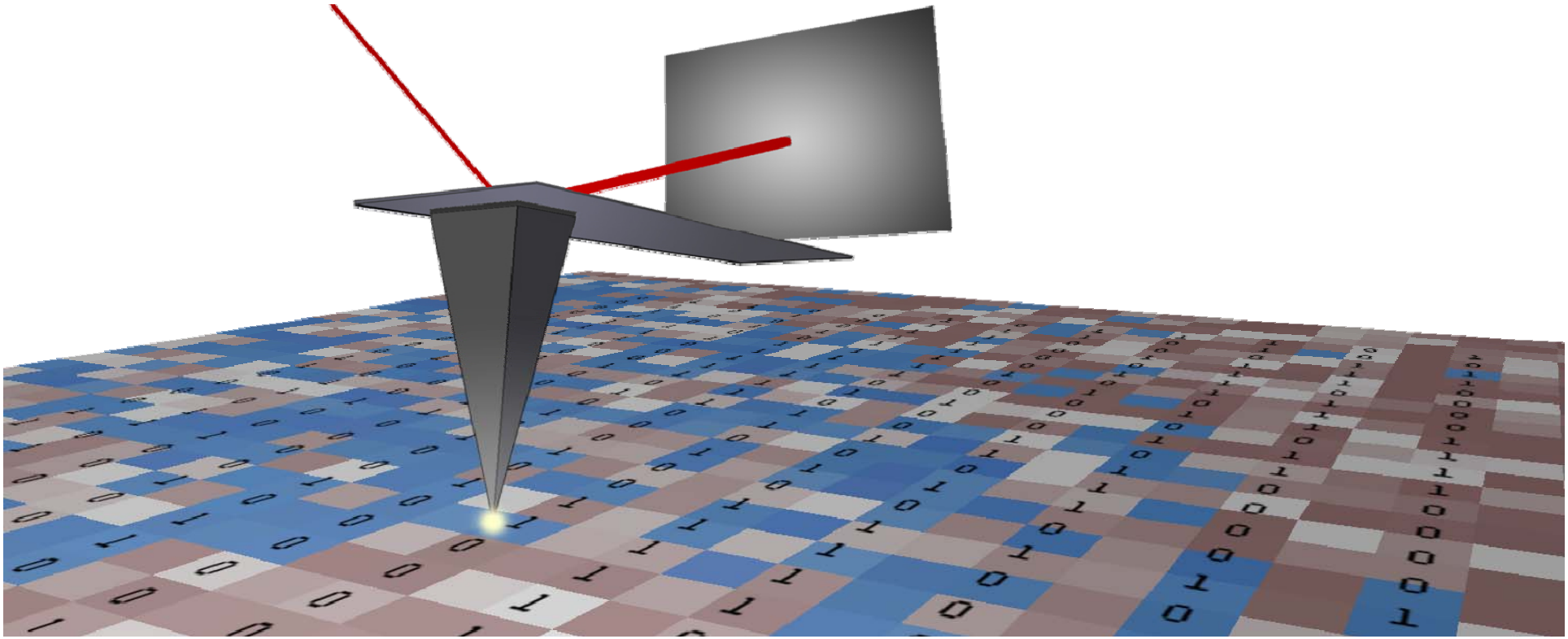

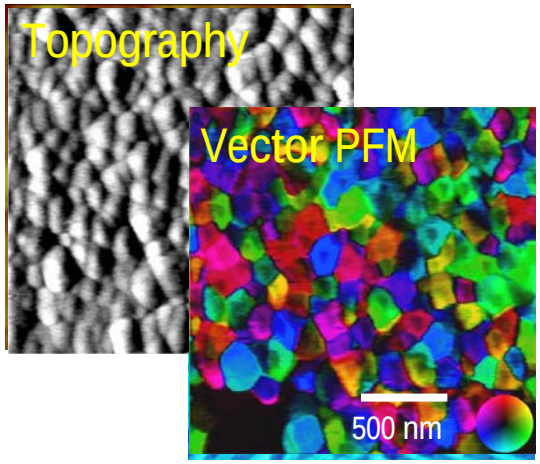

Domain imaging

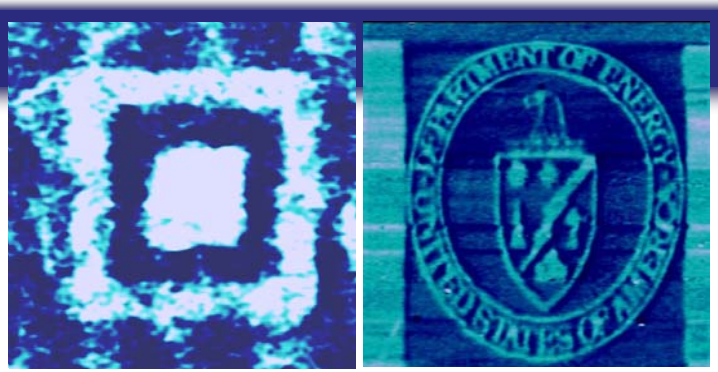

Domain writing

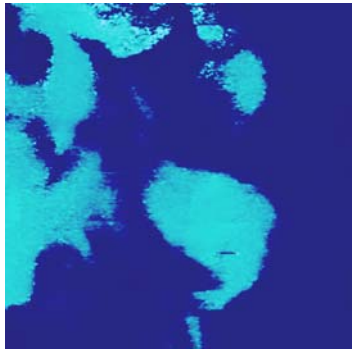

Domain dynamics and evolution

Piezoresponse Force Microscopy

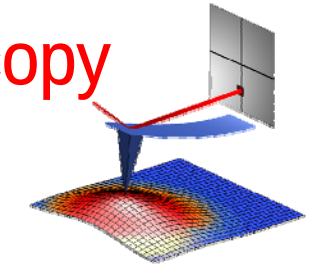

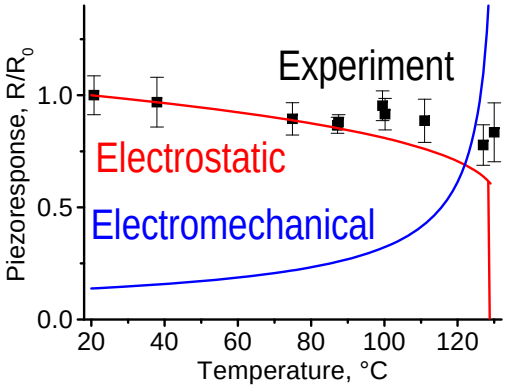

Temperature dynamics and phase transitions

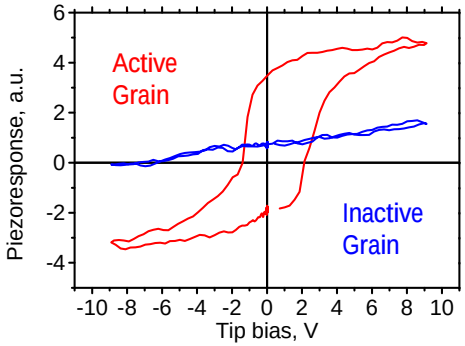

PFM spectroscopy

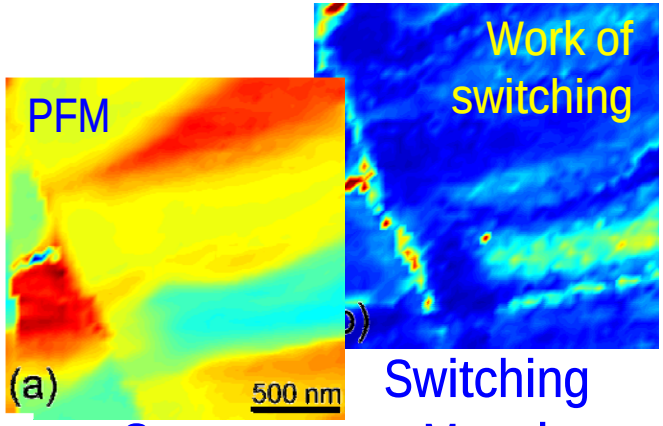

Switching Spectroscopy Mapping

Environmental Effects on PFM and Ferroelectrics

1. Environmental effect on PFM imaging
    - 1.1 Surface conductivity and charge diffusion
    - 1.2. Surface-chemistry controlled polarization stability and imprint
    - 1.3. Tip induced electrochemistry

2. Kelvin Probe Force Microscopy of ferroelectrics
    - 2.1. Charge dynamics on oxide surfaces
    - 2.2. Variable temperature KPFM on ferroelectrics
    - 2.3. Temperature induced potential inversion

3. PFM in Ultra High Vacuum
    - 3.1. Switching mechanisms
    - 3.2. Variable temperature PFM

Transport in Oxide Nanowires

Oxide nanowires can be used as hydrogen sensor, since resistance strongly depends on hydrogen concentration. What is the sensing mechanism – contacts or the wire itself?

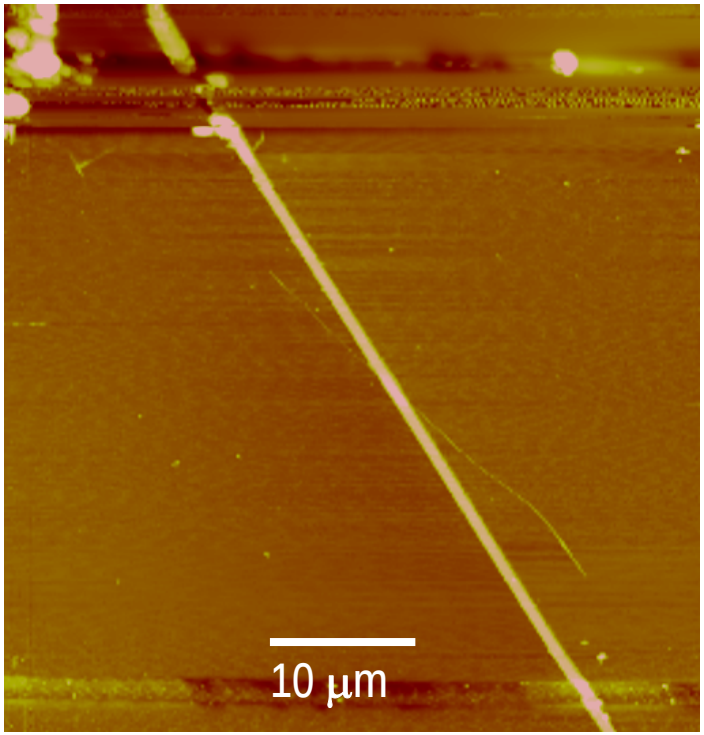

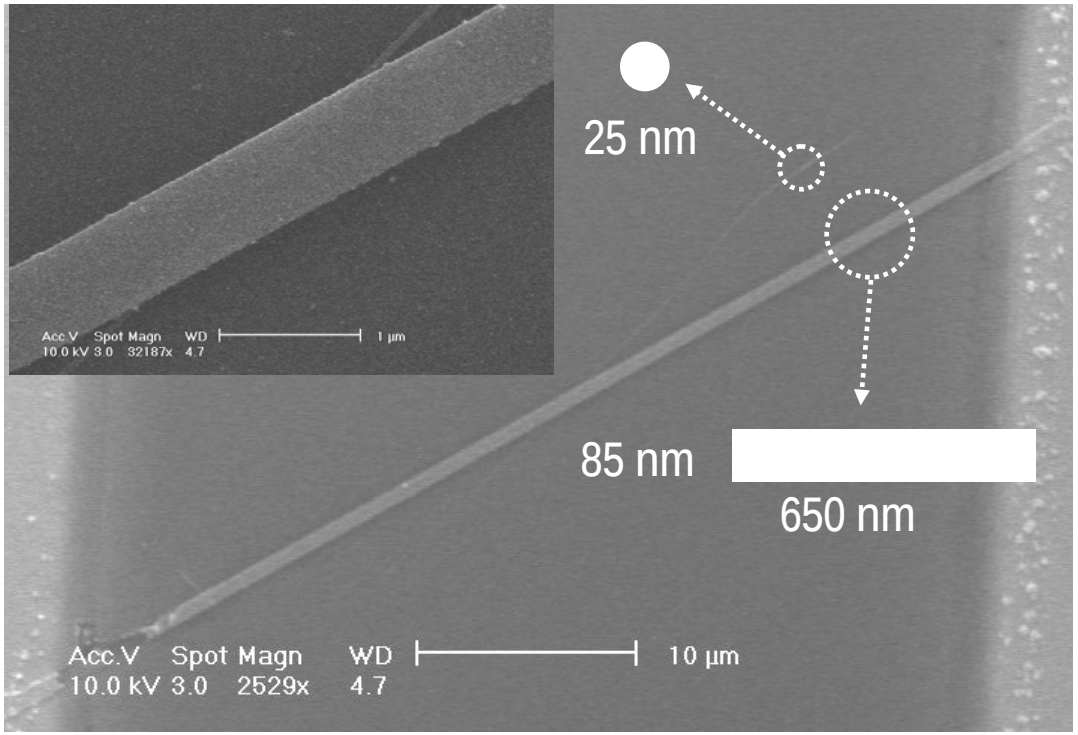

Real Space Imaging of Transport in Nanowires

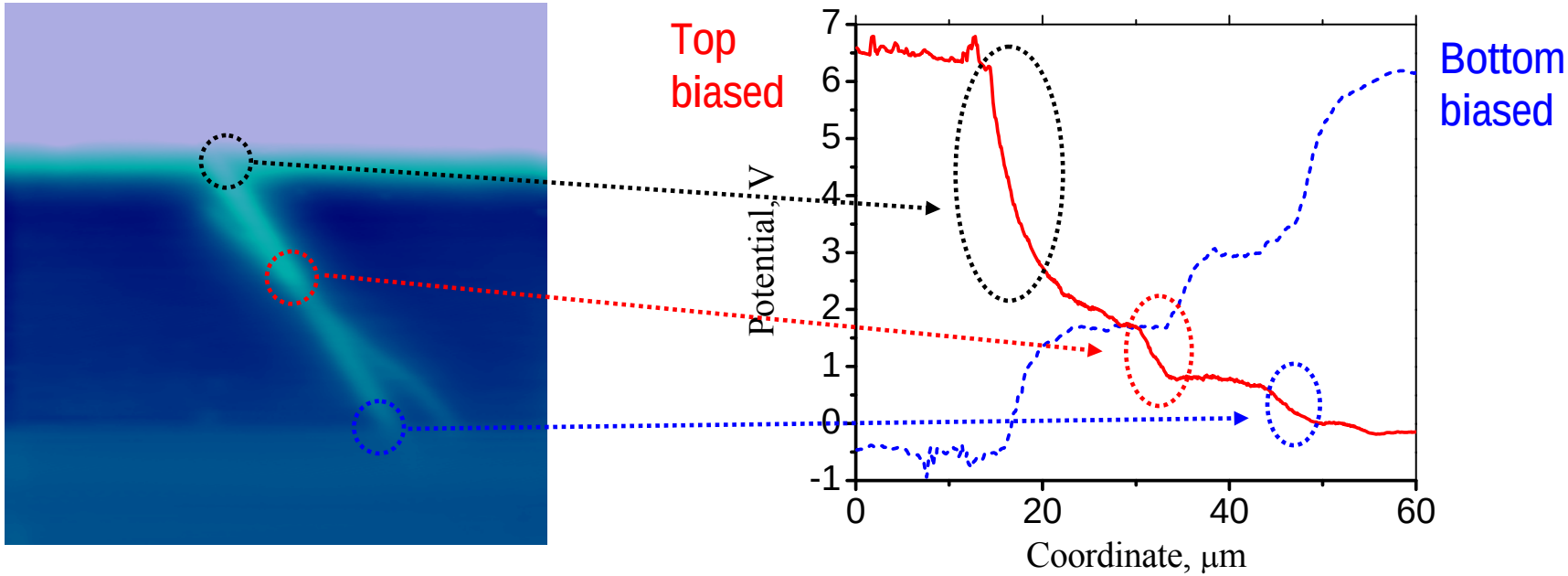

- SPM is used to probe voltage distribution along the nanobelt
- The voltage drops across the individual elements are measured
- Combining with macroscopic I-V data, we determine I-V curve of individual element!

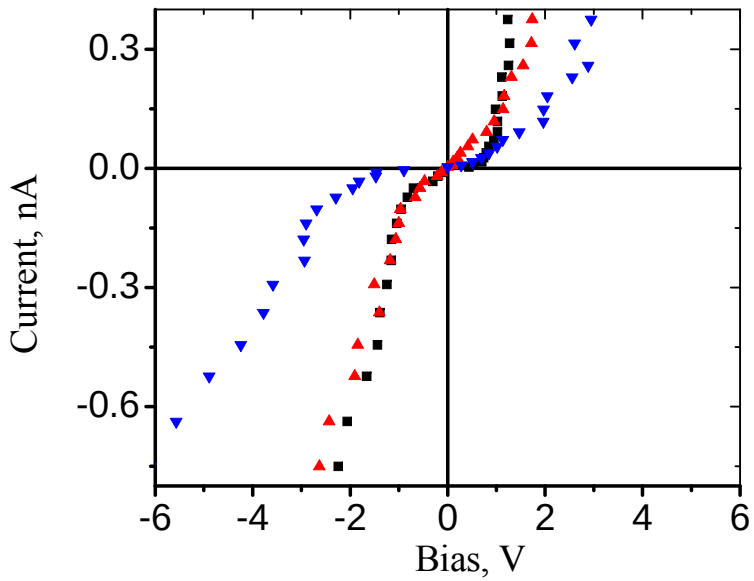

Surface Charging in Ambient Conditions

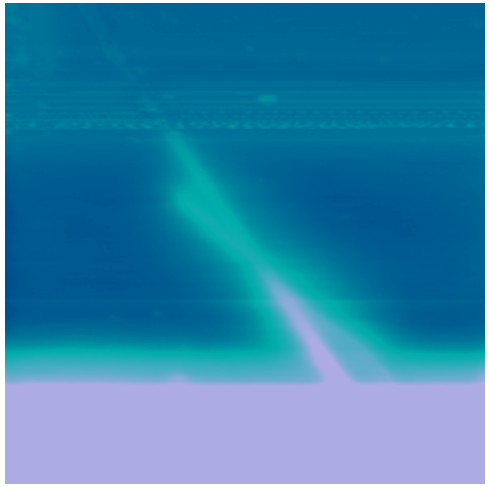

Bias is turned on

Bias is on for 2 hours

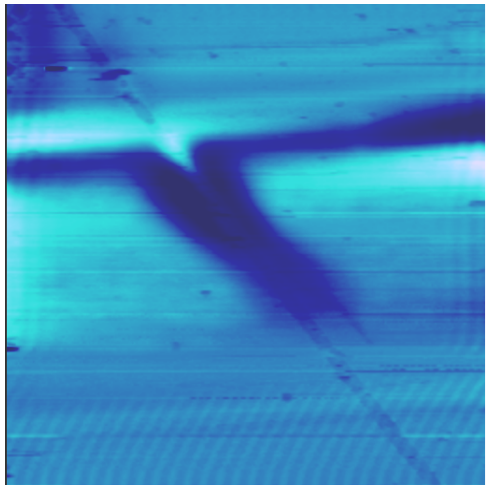

Bias is off

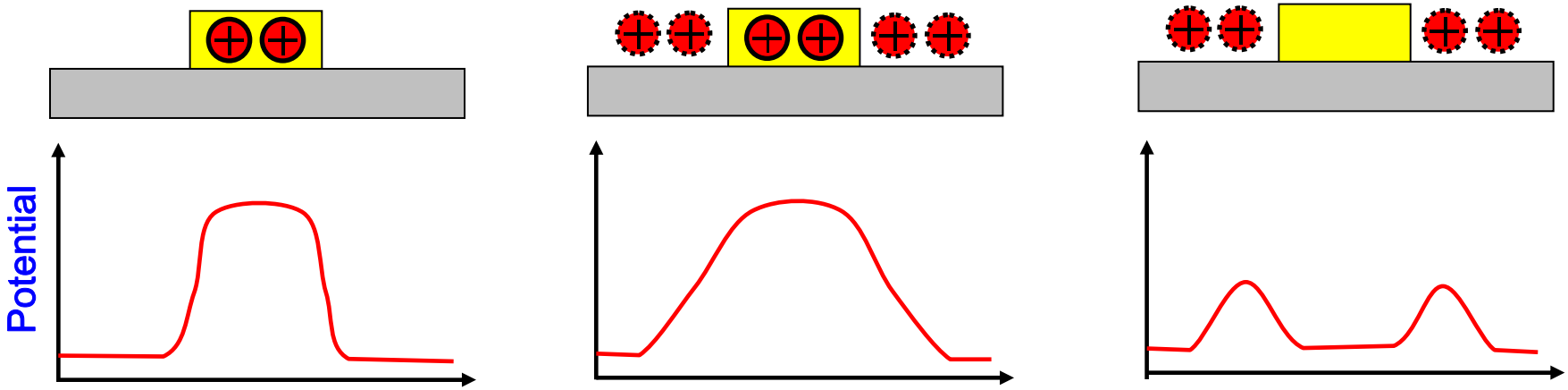

- Surfaces in ambient are covered by water layers containing mobile charges
- Charge redistribute slowly under the action of electric field
- This phenomenon is materials and environment specific:
  - Rainy day in Tennessee is worse than sunny day in Albuquerque

Limits of SPM based Transport Imaging

The key problems:

1. Tip state (stability)
2. Environmental effects
3. Capillary and VdW forces:
   - limit contact area
4. Non-local electrostatic interactions:
   - linear contribution to signal
5. Input impedance of electrometer/shielding

1. Sign inversion of grain boundaries
2. Temperature induced potential inversion in ferroelectrics
3. Potential retention above phase transition in ferroelectrics
4. Charge migration under bias

But: relaxation times: ~10 minutes
Matters only to dc probes

Solutions

1. Environment
   - controlled atmosphere
   - UHV
2. Better probes
   - shielding (force- and current based techniques)
   - stable (resolution, reproducibility, quantitativeness)

Nanostructure Fabrication by Nanooxidation

Even small biases create huge electric fields!

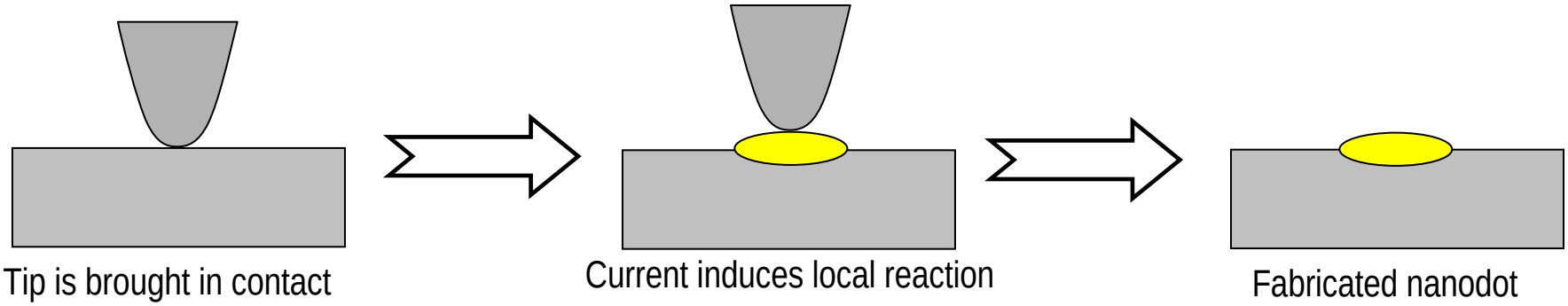

Local electrochemical reaction is usually mediated by water meniscus: $Si + 2H_2O + 4h^{\cdot} \rightarrow SiO_2 + 4H^+$

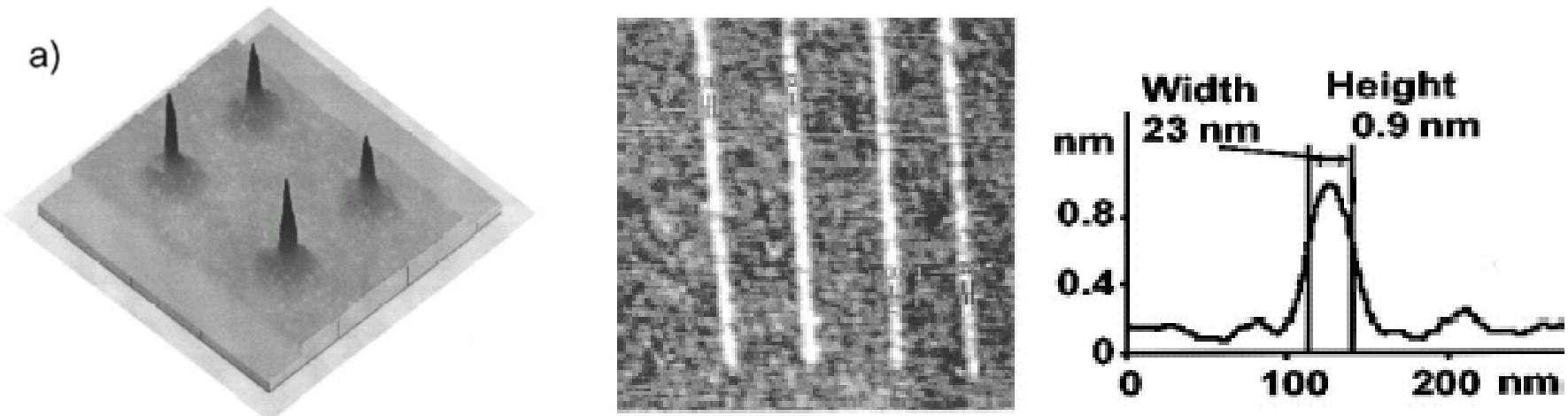

SiO_2 nanodots and nanolines fabrication using NC-AFM based nanooxidation
Same approach can be used to multiple materials – e.g. Zr, Ti, GaAs, etc.

N. Clements et al., J. Vac. Sci. Technol. B 21, 2348 (2003)

Resist Method

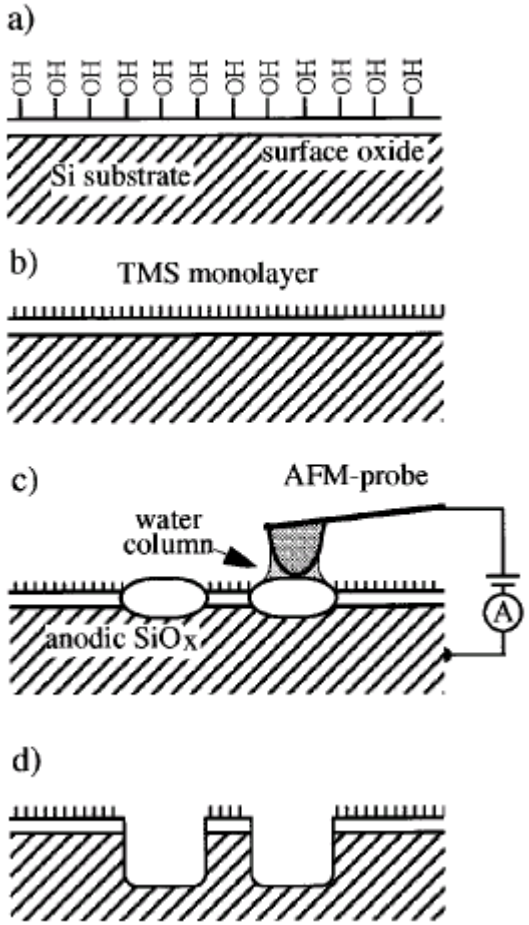

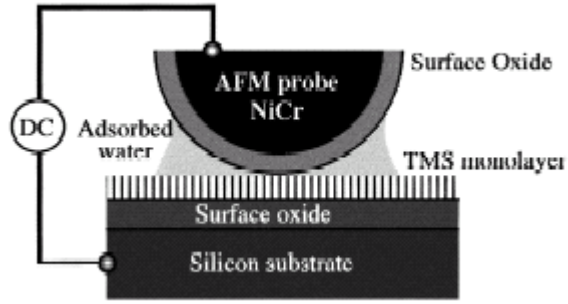

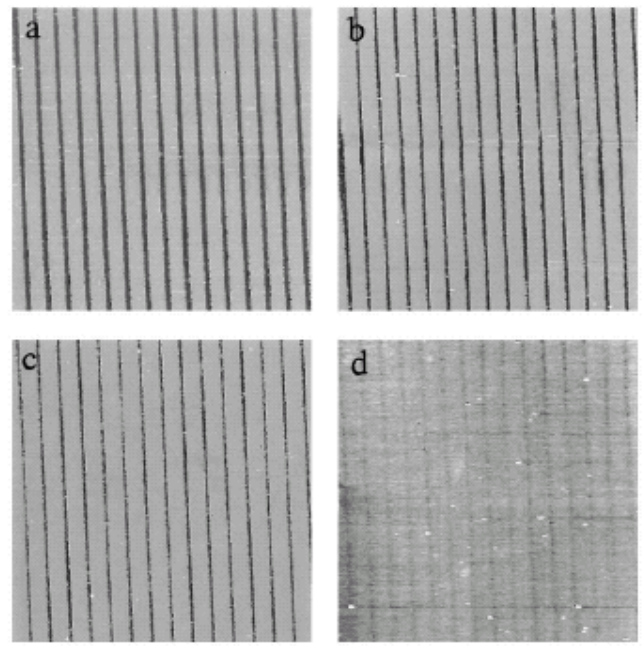

Schematics of resist-based electrochemical nanooxidation

AFM images of etched grooves on a Si substrate showing the dependence of the AFM-induced degradation rate on probe scan rate. (a) 20 μm/s, (b) 80 μm/s, (c) 160 μm/s, and (d) 400 μm/s. The size of each image is 10x10 μm2.

H. Sugimura et al, J. Vac. Sci. Technol. B 14, 4140 (1996).

Environmental Effects in PFM

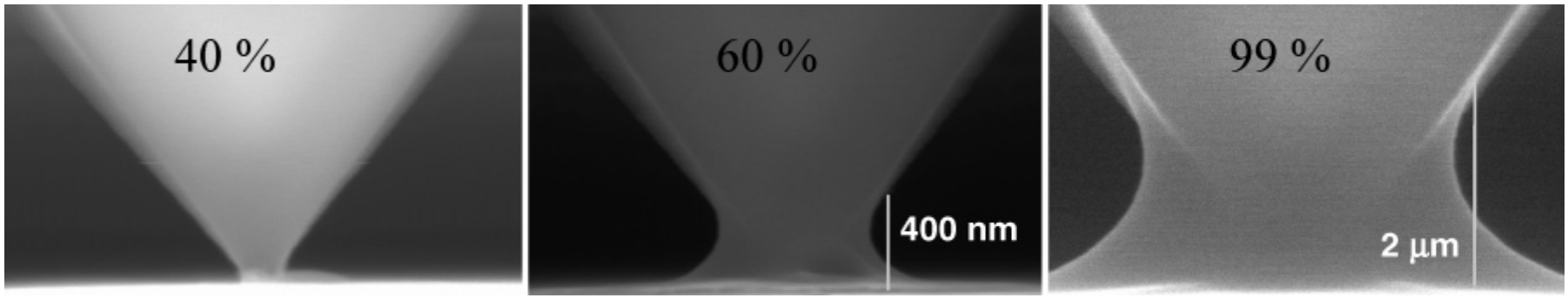

- There is a meniscus at the tip-surface junction
- The 2D diffusion gives rise to similar kinetic laws

Langmuir 21, 8096-8098 (2005)

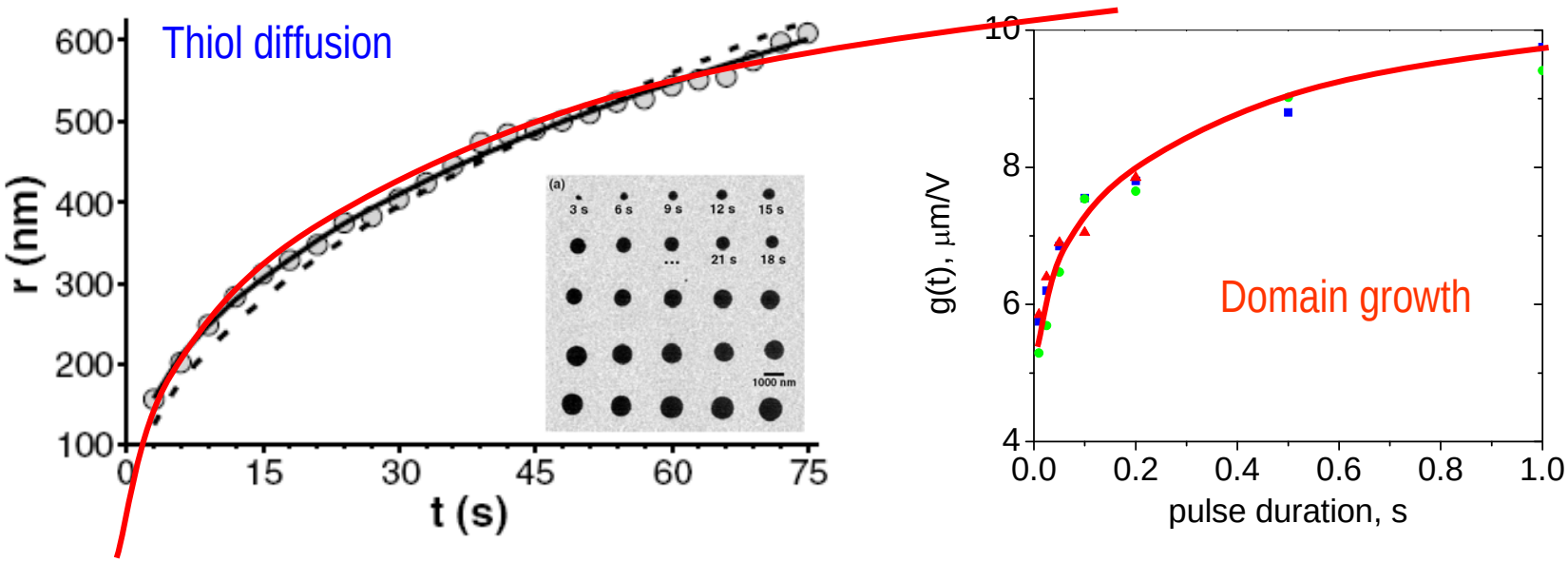

P. E. Sheehan, L. J. Whitman, W.P. King, and B.A. Nelson, Appl. Phys. Lett. 85, 1589 (2004)

Adsorbed Water Effects on PFM

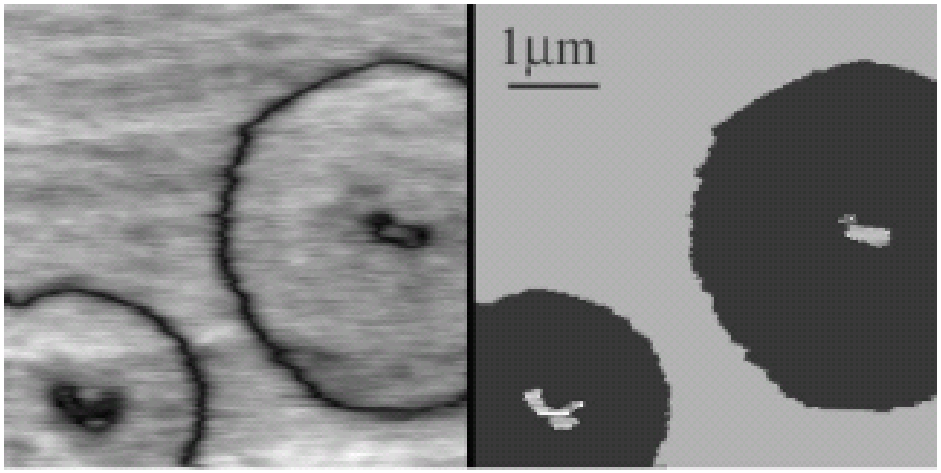

S. Bühlmann, E. Colla, and P. Muralt,
Polarization reversal due to charge injection in ferroelectric films,
Phys. Rev. B 72, 214120 (2005)

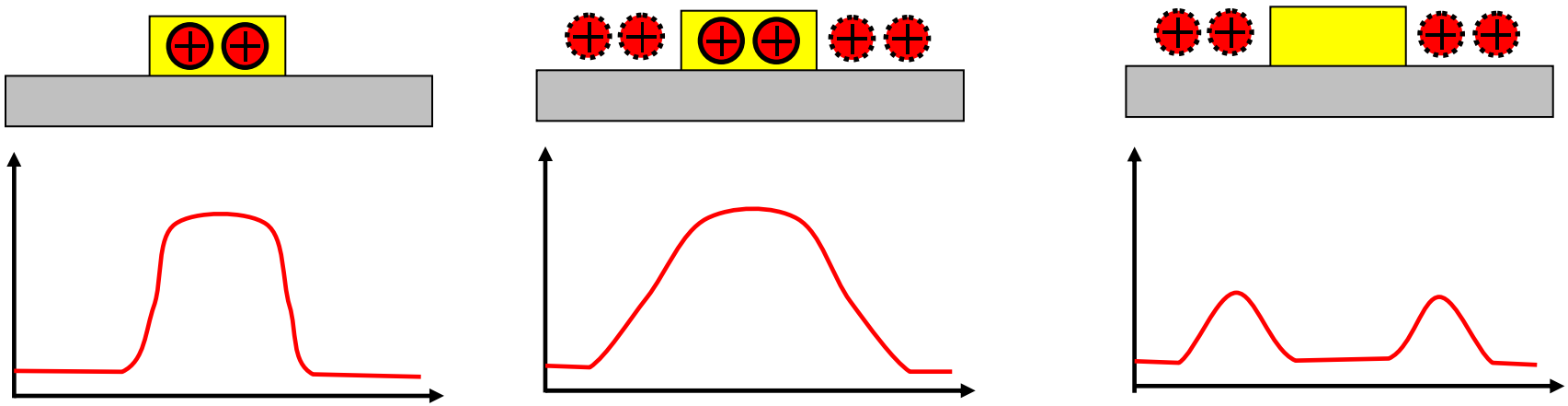

Formation of “bubble” domains, previously attributed to ferroelectroelastc switching, is actually due to surface charge dynamics!

Domain Relaxation Kinetics

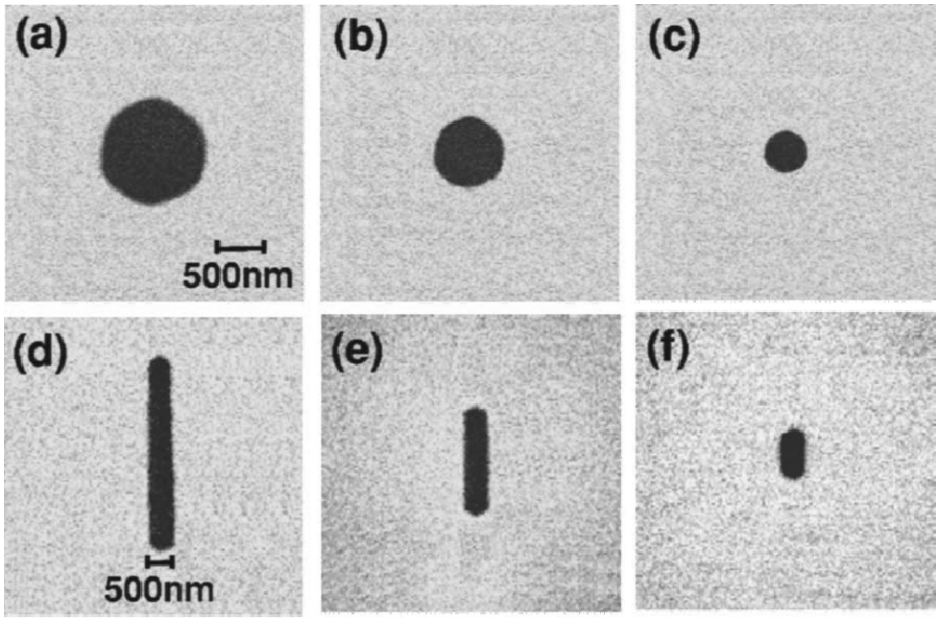

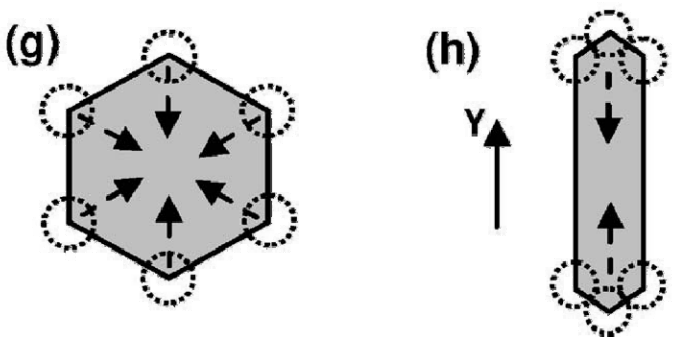

- Domain relaxation is driven by the corners
- Relaxation can be fast at high temperatures
- Relaxation depends on the screening processes (air vs. vacuum)
- Relaxation can be minimized by increasing density of pinning sites – e.g. by ion implantation

X. Liu, K. Kitamura, and K. Terabe, Appl. Phys. Lett. 89, 142906 (2006).

Surface Chemistry Effects on PFM

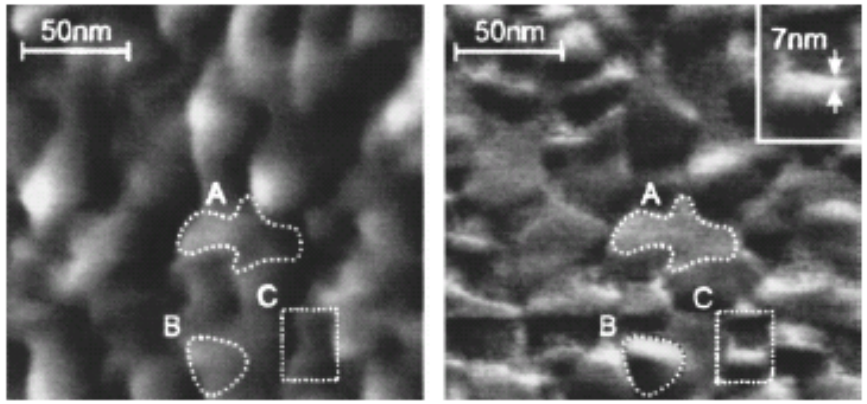

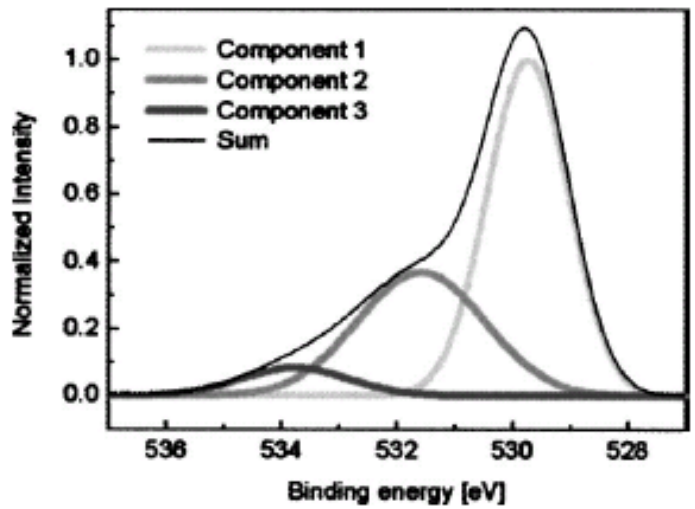

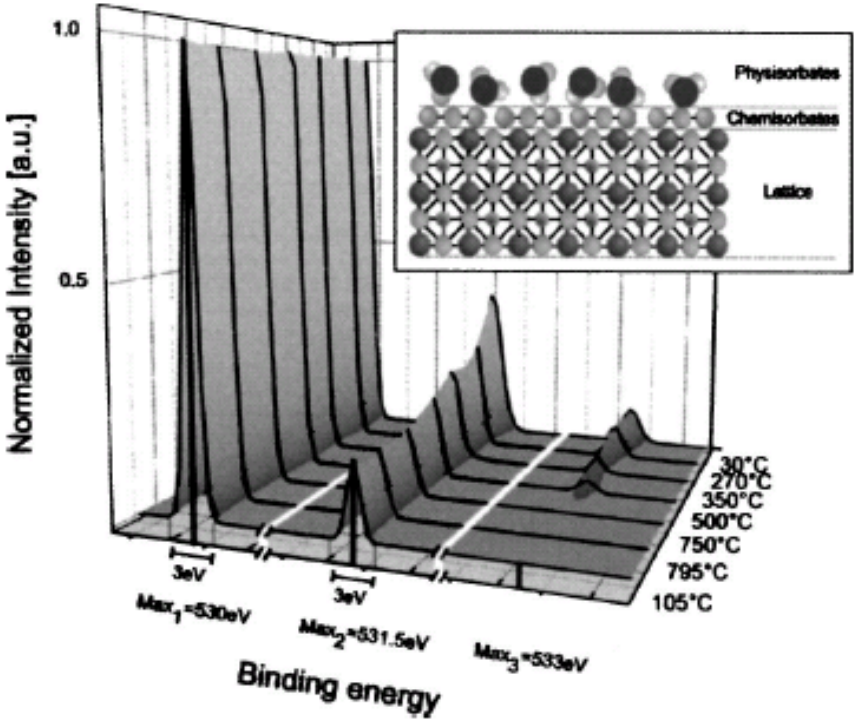

F. Peter, K. Szot, R. Waser, B. Reichenberg, S. Tiedke, and J. Szade,
Piezoresponse in the light of surface adsorbates: Relevance of defined surface conditions for perovskite materials,
Appl. Phys. Lett. 85, 2896 (2004)

Theoretical Studies

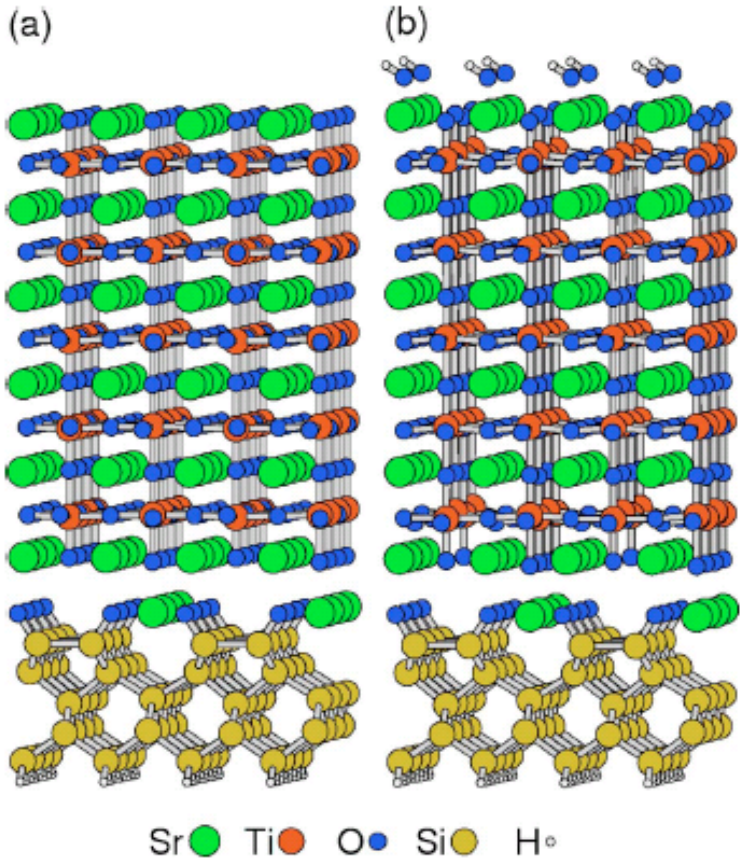

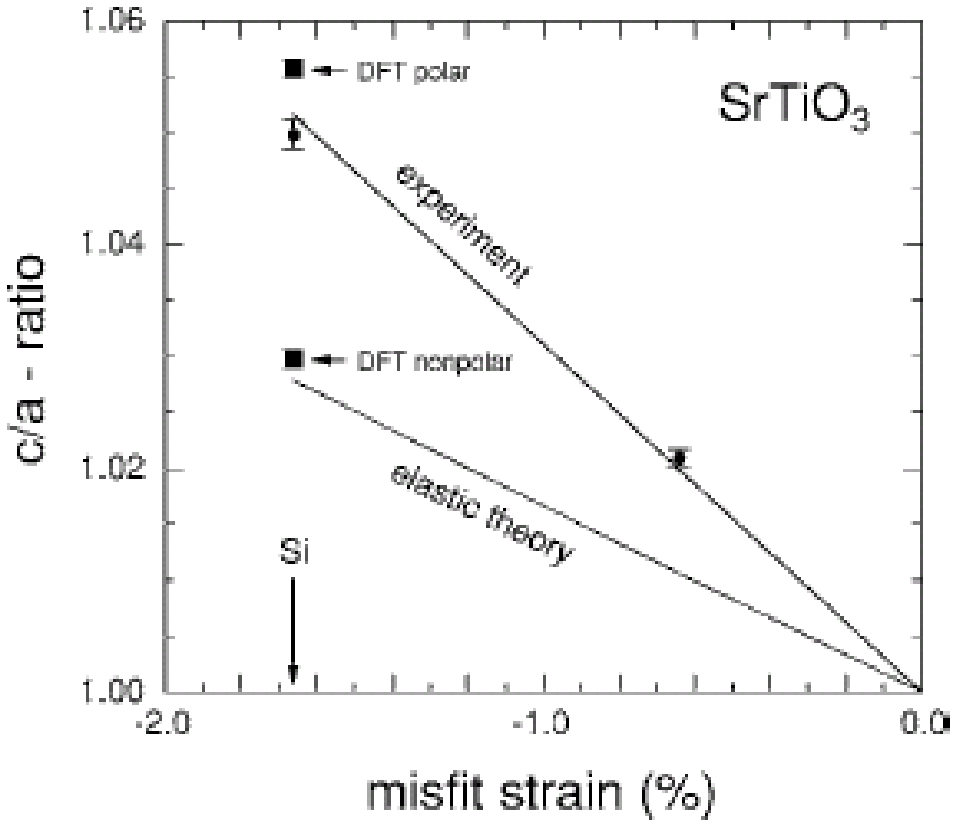

J.C. Woicik, H. Li, P. Zschack, E. Karapetrova, P. Ryan, C. R. Ashman, and C. S. Hellberg, Anomalous lattice expansion of coherently strained SrTiO3 thin films grown on Si (001) by kinetically controlled sequential deposition, Phys. Rev. B 73, 024112 (2006)

Theoretical Studies

TABLE I. Polarization and ΔE_{DFT} from DFT calculations, with estimated reaction energies per adsorbate at $T = 300$ K.

Adsorbate	$P/\lvert P_{bulk}\rvert$	ΔE_{DFT} (eV)	ΔH^0 (eV)	ΔG^0 (eV)	ΔG (eV)
OH	0.7	−2.00	−2.34	−1.96	−0.20
O	0.9	−0.92	−0.95	−0.52	1.95
H	−0.8	−2.90	−2.93	−2.65	0.79

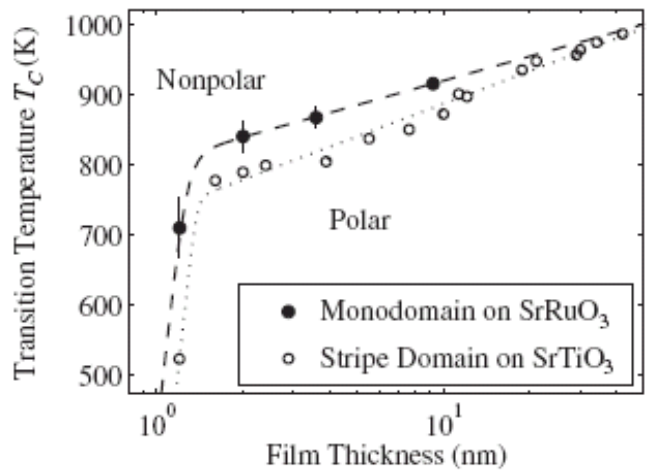

D. D. Fong et al., Stabilization of Monodomain Polarization in Ultrathin PbTiO3 Films, Phys. Rev. Lett. 96, 127601 (2006)

V-PFM (13 nm PZT thin films)

Reading image after writing image (5 μm size)

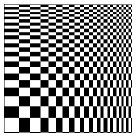

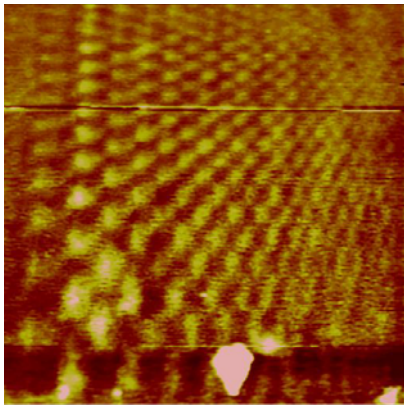

Topography
Scan 5 μm, scale 5 nm

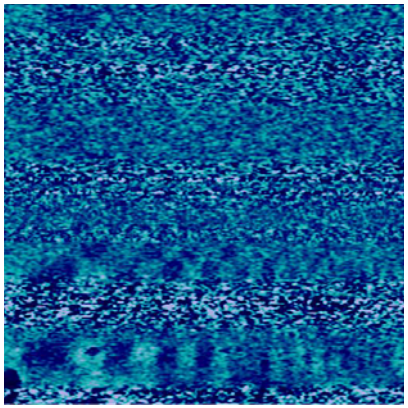

amplitude, scale 500 mV

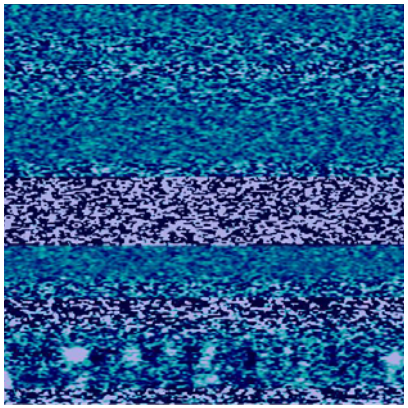

phase, scale 1 V

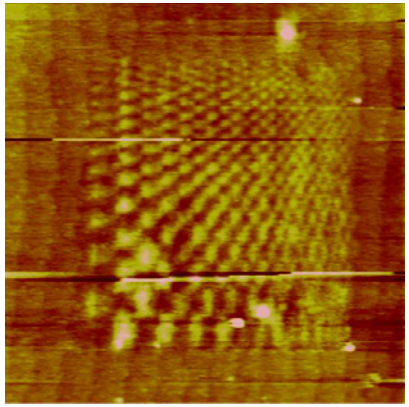

Topography

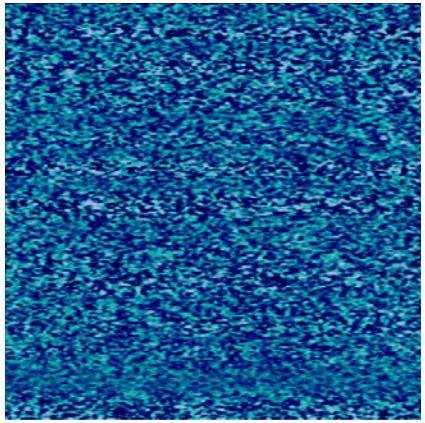

amplitude, scale 500 mV

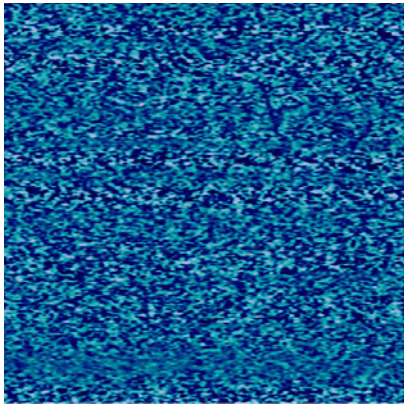

phase, scale 1 V

Reading image after writing image (5 μm size).

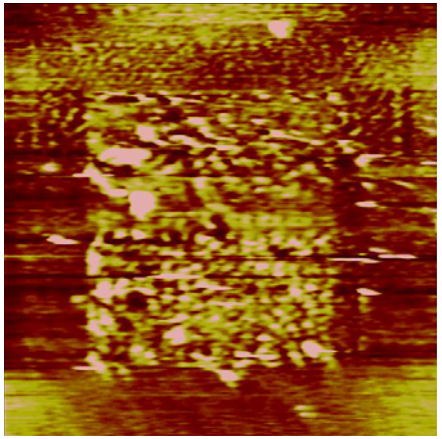

Topography
Scan 8 μm, scale 5nm

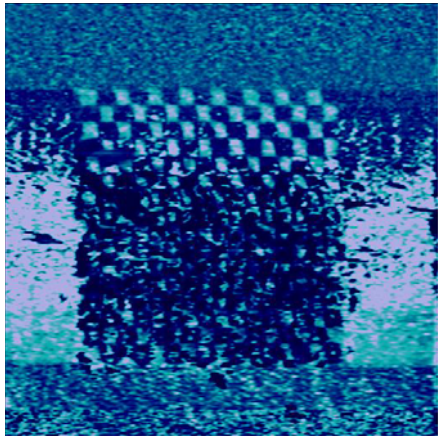

amplitude, scale 1 V

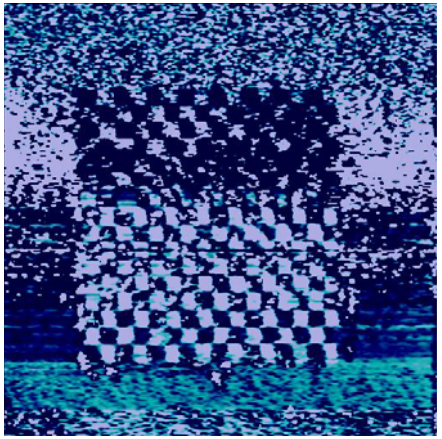

phase, scale 2 V

Reading image after writing image (3 μm size).

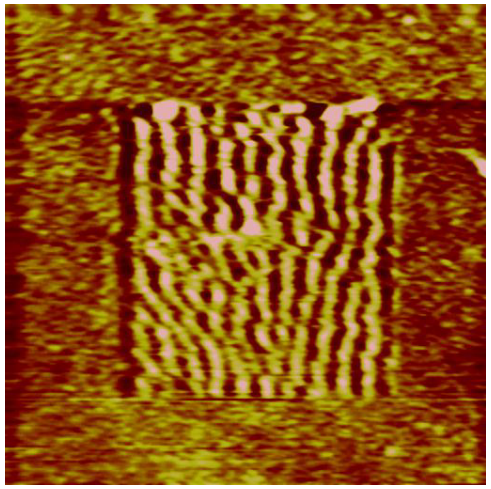

Topography
Scan 5 μm, scale 5nm

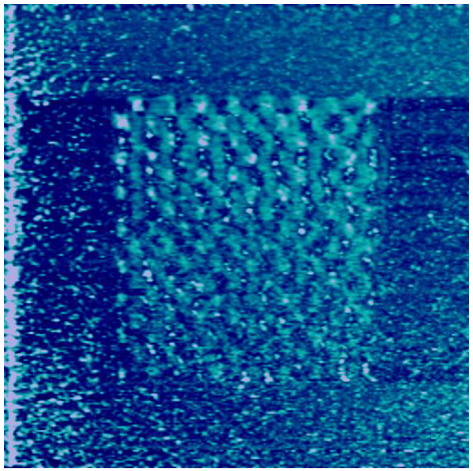

amplitude, scale 1 V

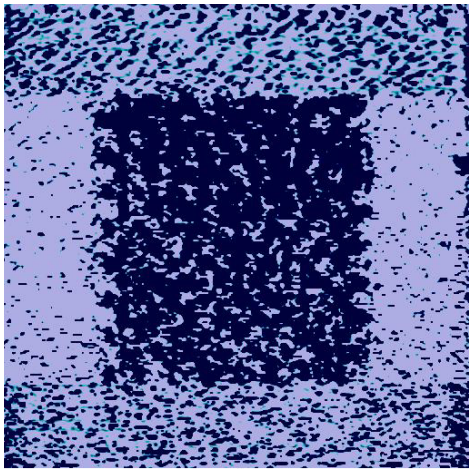

phase, scale 2 V

Reading image after writing image (2 μm size).

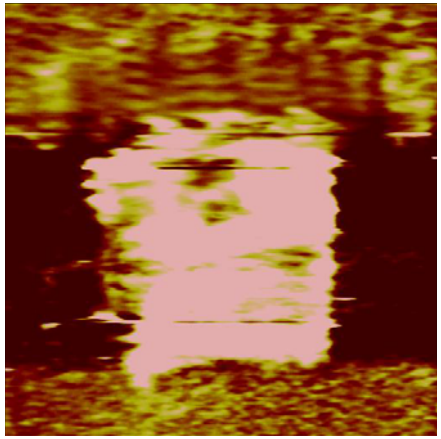

Topography
Scan 4 μm, scale 5nm

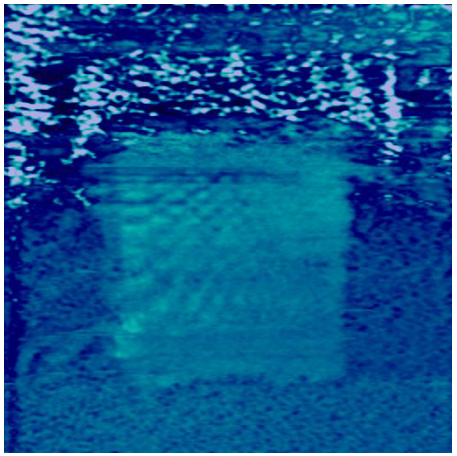

amplitude, scale 1 V

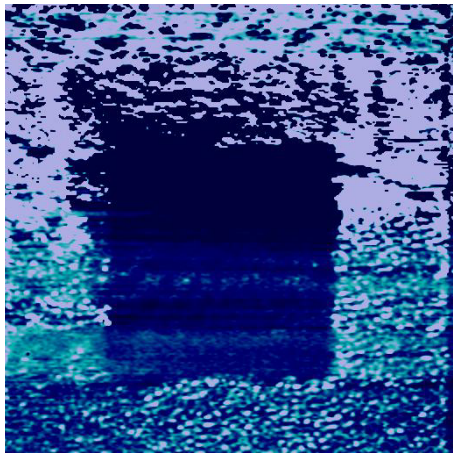

phase, scale 2 V

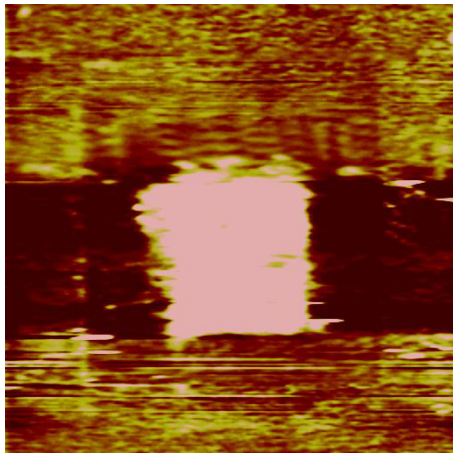

Topography
Scan 6 μm, scale 5nm

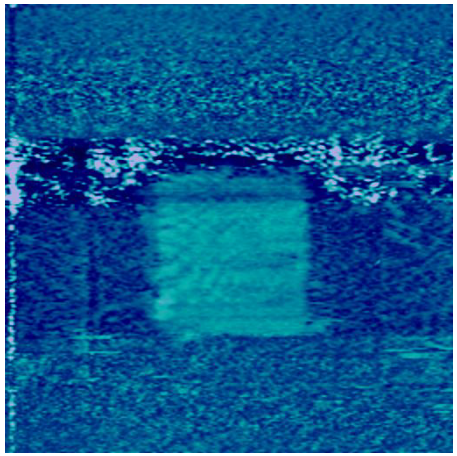

amplitude, scale 1 V

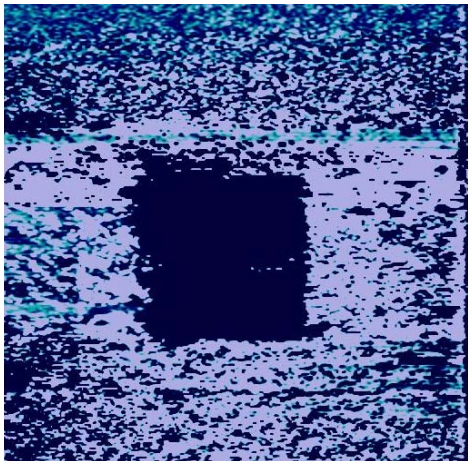

phase, scale 2 V

Scanning Surface Potential Microscopy

SSPM is also known as Kelvin Probe Force Microscopy (KPFM)

$$V_{tip} = V_{dc} + V_{ac}\cos\omega t$$

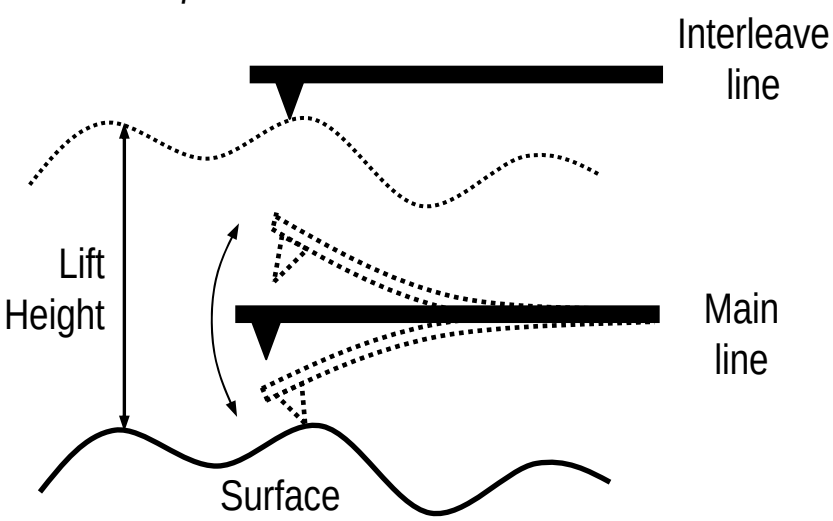

Cantilever response (no feedback):

$$d = d_0 + A(\omega)\cos(\omega t + \varphi)$$

Capacitive force:

$$F = \frac{1}{2}\frac{dC}{dz}(V_{tip} - V_{surface})^2$$

First harmonic of the force:

$$F_{1\omega} = \frac{dC}{dz}V_{ac}(V_{dc} - V_{surface})$$

Feedback: $F_{1\omega} = 0 \Rightarrow V_{dc} = V_{surface}$

For ideal feedback:

Signal is independent of phase φ and magnitude $A(\omega)$ of response

Domain Structure in Ferroelectric Materials

Polarization in $BaTiO_3$ develops along one of the six (100) directions

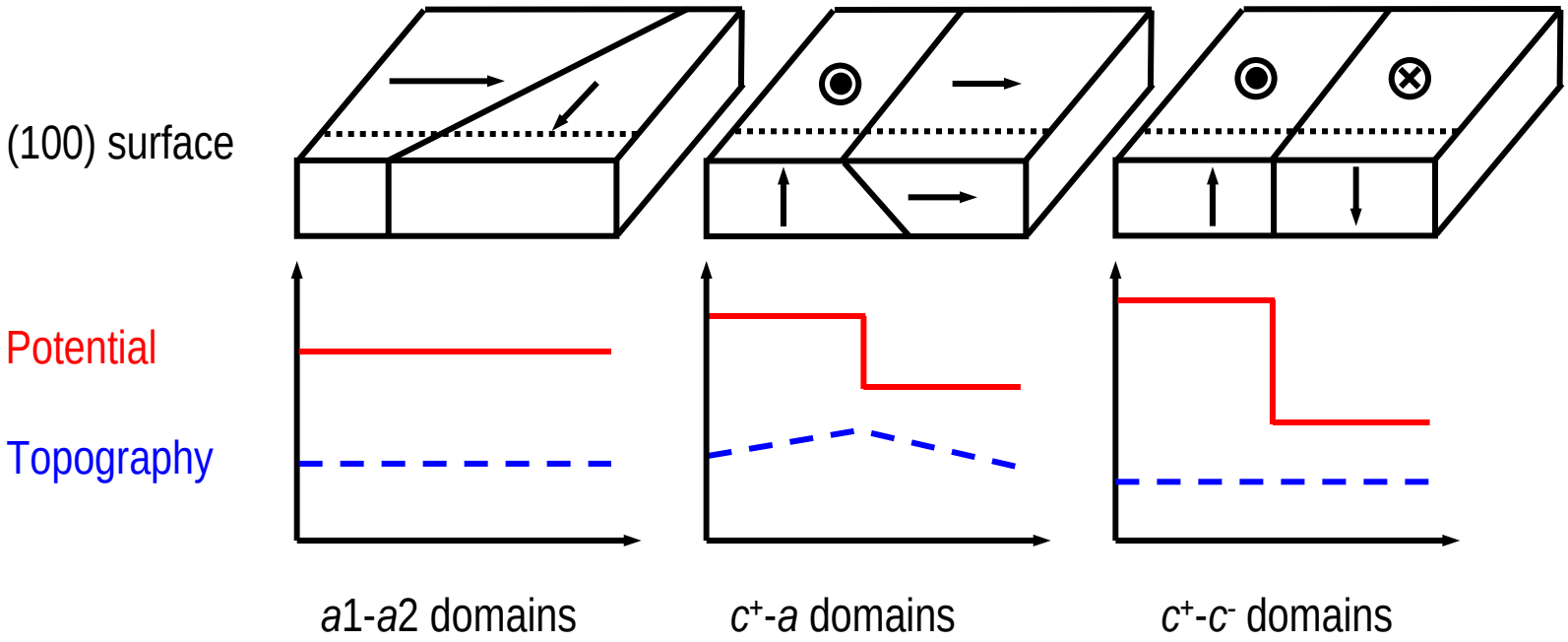

Domain structure:

1. Hysteresis and switching
2. Fatigue
3. Non-volatile memories
4. Ferroelectric heterostructures

Polarization discontinuities: Charge $\sigma_{pol} = P \cdot n$

Typical value: 0.26 C/m^2 ~ 0.26 e^-/u.c.

In traditional measurements, surface properties of ferroelectric materials are usually averaged over domain orientations.

Domain Imaging in Ferroelectric Materials

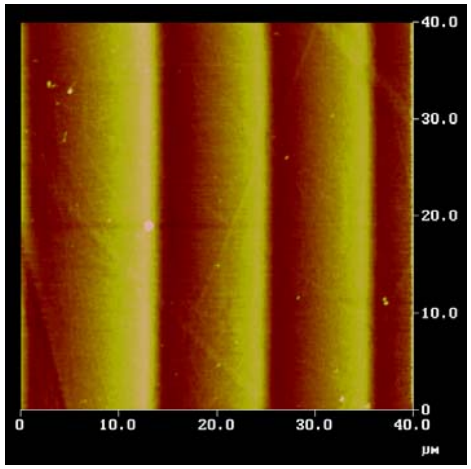

Topography

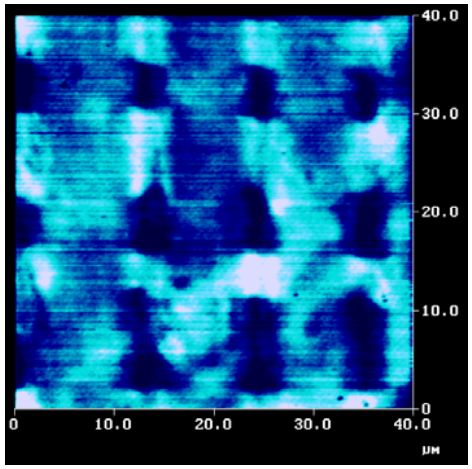

Surface potential

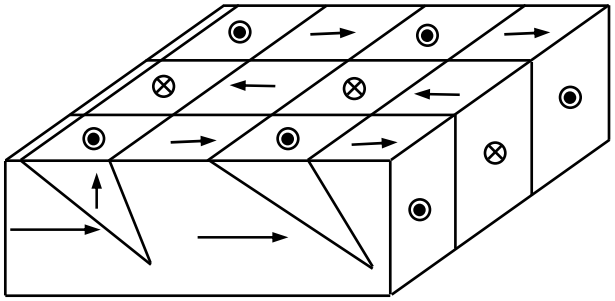

Domain structure is formed by *c*-domain wedges in preferentially *a*-domain material

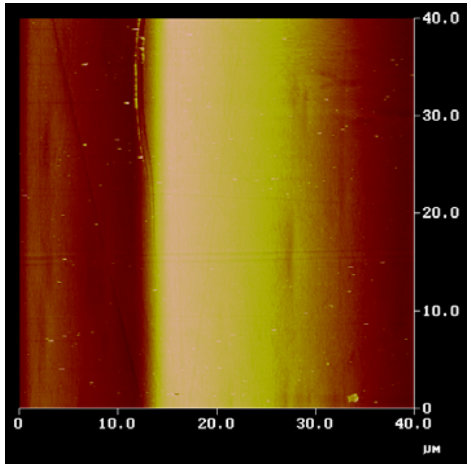

Topography

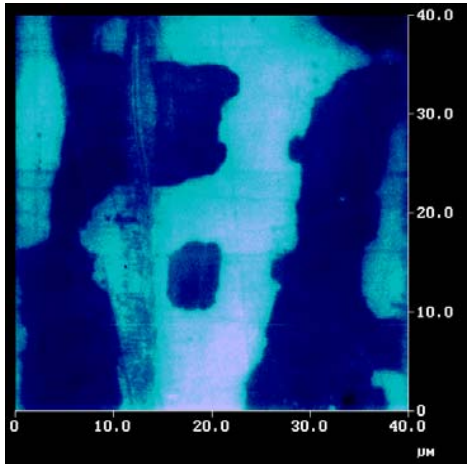

Surface potential

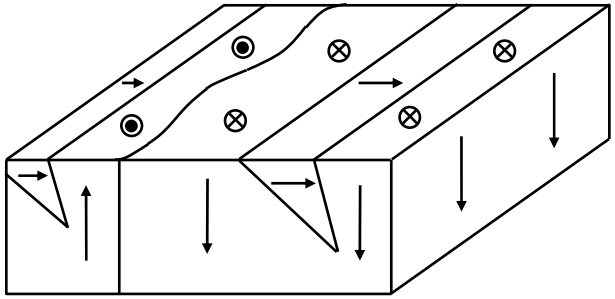

Domain structure is formed by *a*-domain wedges in preferentially *c*-domain material

Effective potential difference between domains of opposite polarity is $\Delta V \approx 150$ mV

Variable Temperature SPM

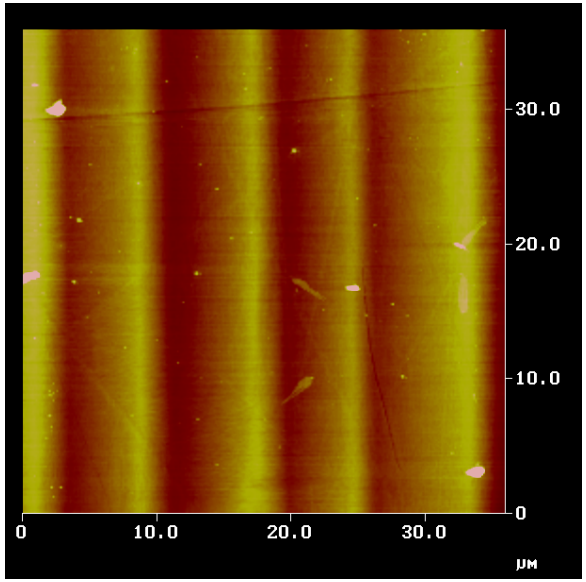

Topography

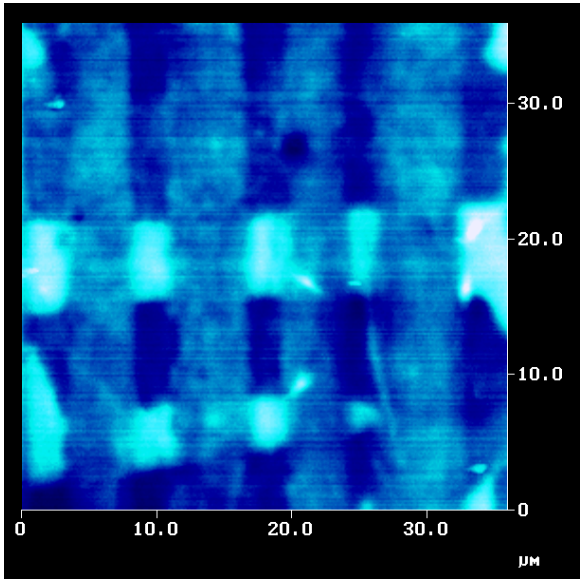

Surface potential

1. Image formation mechanism in SPMs on ferroelectric materials
2. Dynamic behavior of ferroelectric domain structure

In-situ imaging of Phase Transition

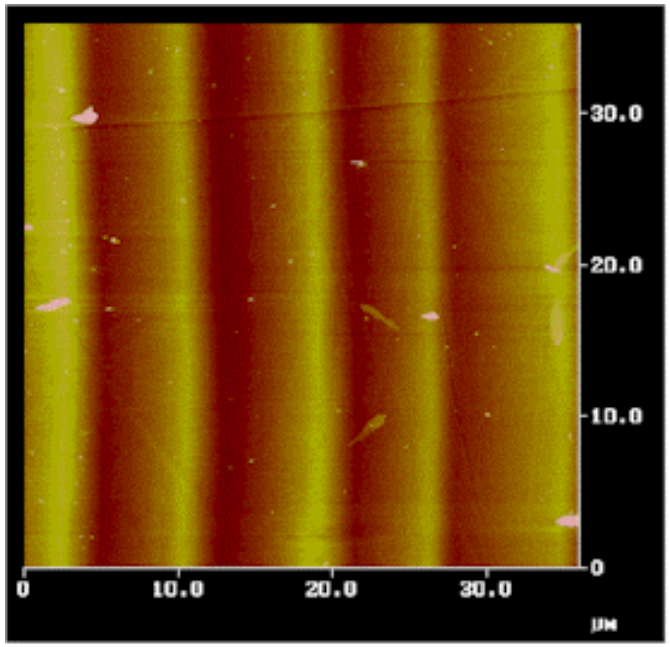

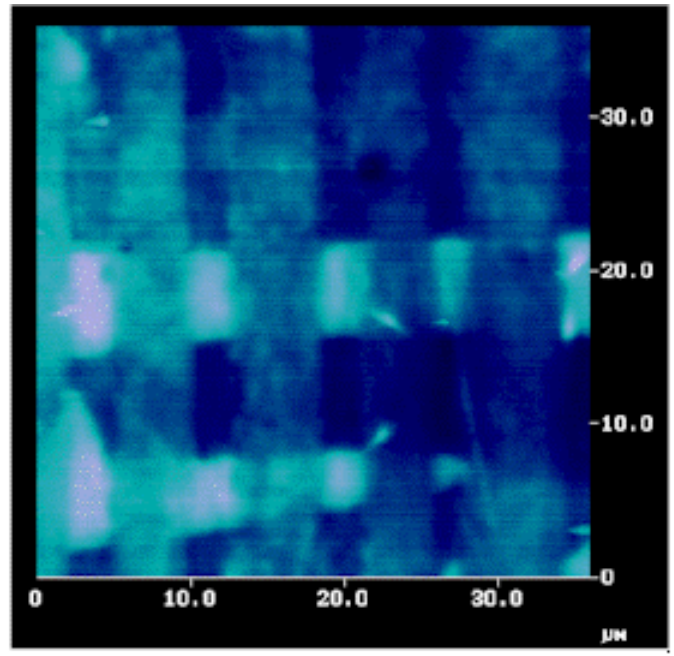

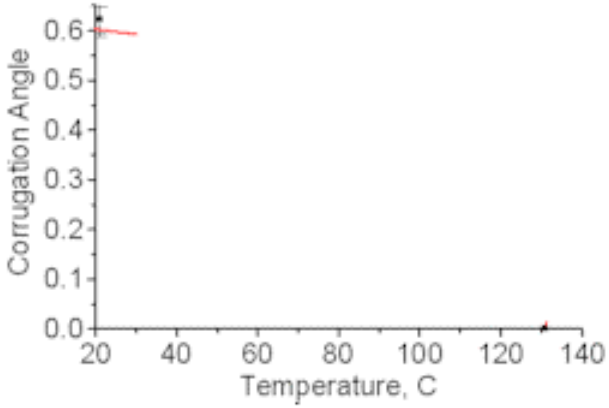

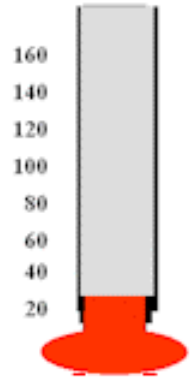

Interpretation of AFM and SSPM Results

Potential behavior during ferroelectric phase transition indicates that the sign of domain potential is reverse to that expected from polarization charge. c^+ domains are negative and c^- domains are positive.

Before the transition

Polarization charge is completely compensated

Surface potential is opposite in sign to polarization charge

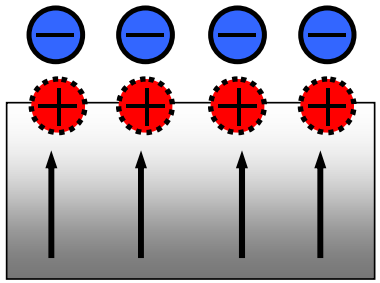

After transition

Polarization disappears; screening charge is uncompensated

Surface potential retains sign and increases in magnitude

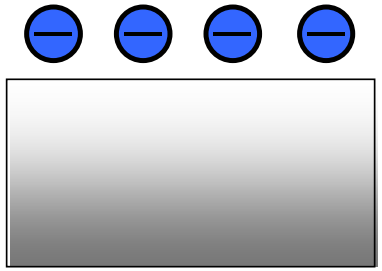

After annealing

Screening charge dissipates

Domain related potential features disappear

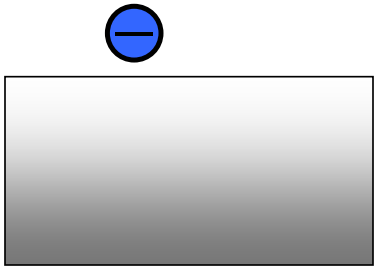

Temperature Induced Domain Potential Inversion

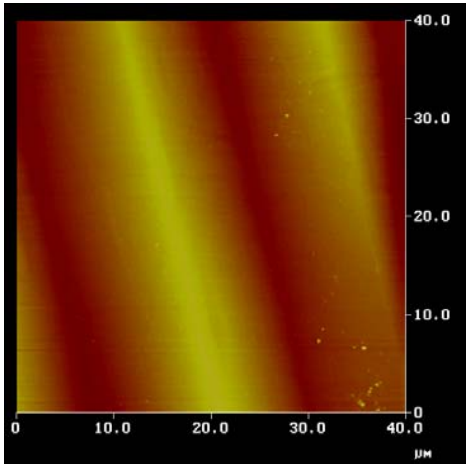

Topography at T = 90°C

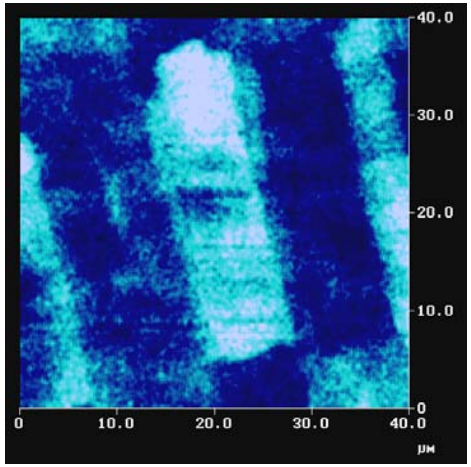

Potential at T = 90°C

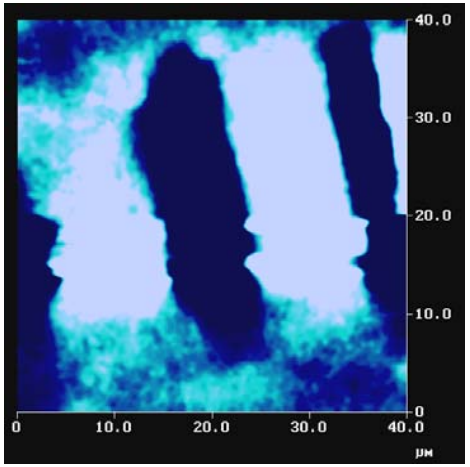

From 90°C to 70 °C

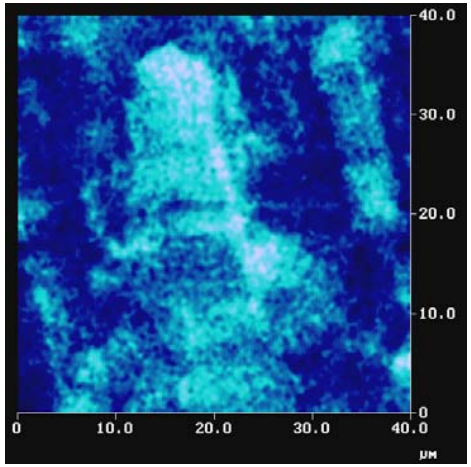

T = 70°C, 10 min

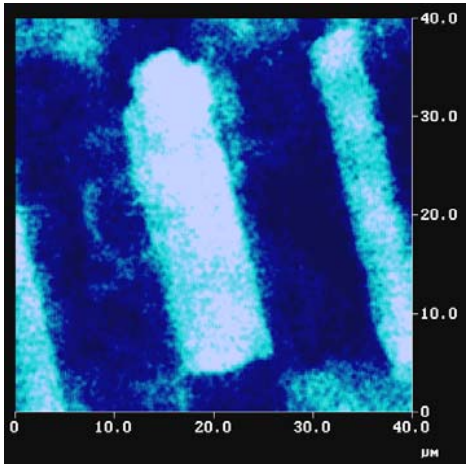

T = 70°C, 1 h

Kinetics of Potential Relaxation

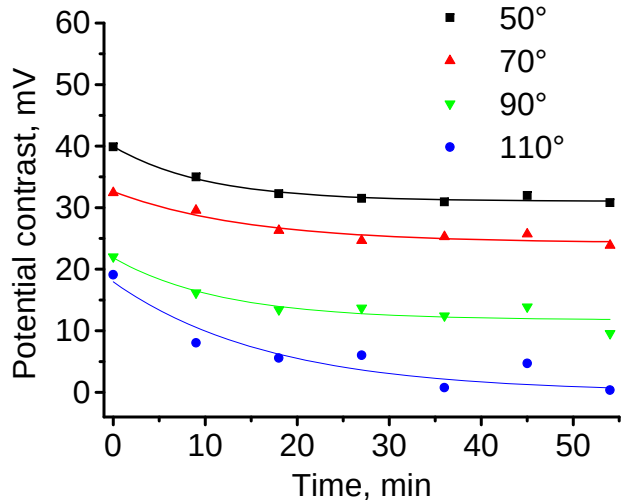

Time dependence of domain potential contrast on heating

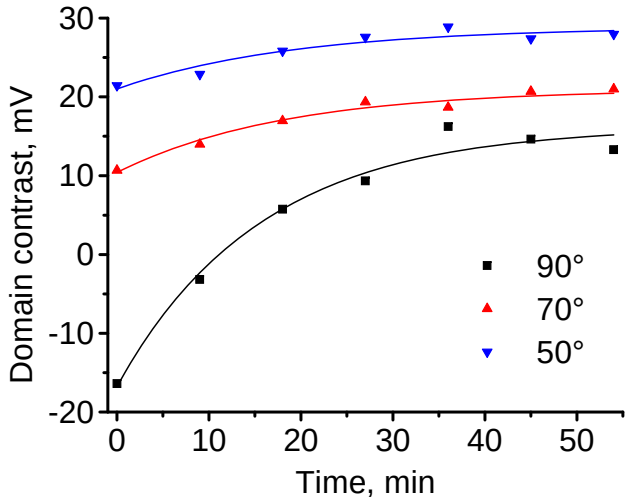

… and cooling

$$\Delta\varphi = \Delta\varphi_0 + A\exp(-t/\tau)$$

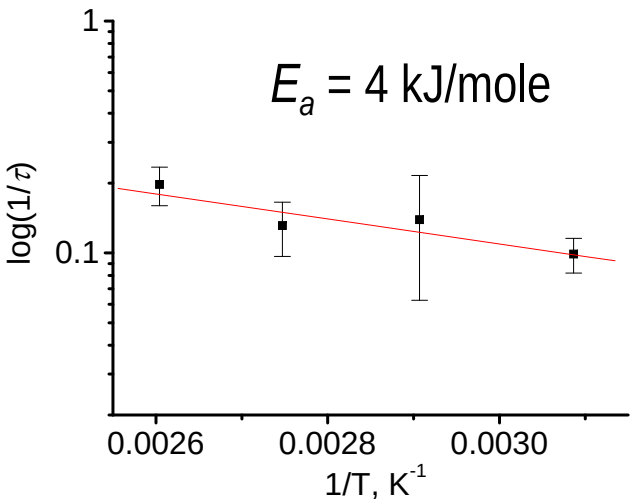

Arrhenius plot for relaxation time

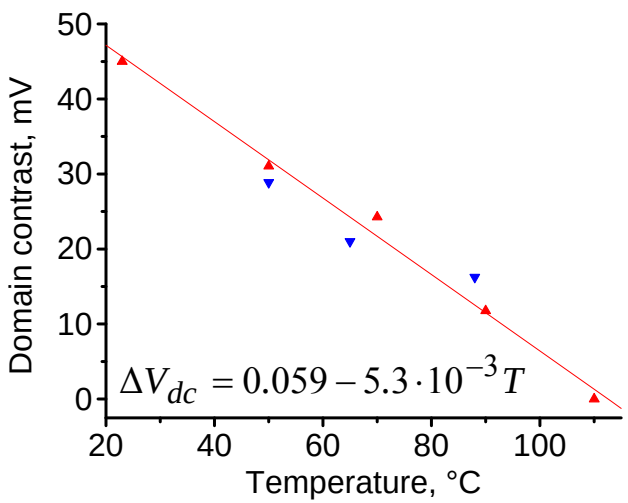

Temperature dependence of equilibrium surface potential

Thermodynamics and Kinetics of Screening Process

Degree of screening: $\alpha = -\sigma_{sc}/P\cdot n$

Free energy for adsorption process:

$$E(\alpha,T) = E_{el}(\alpha,T) + \alpha\frac{P}{qN_a}\Delta H_{\text{ads}} - \alpha\frac{P}{qN_a}T\Delta S_{\text{ads}}$$

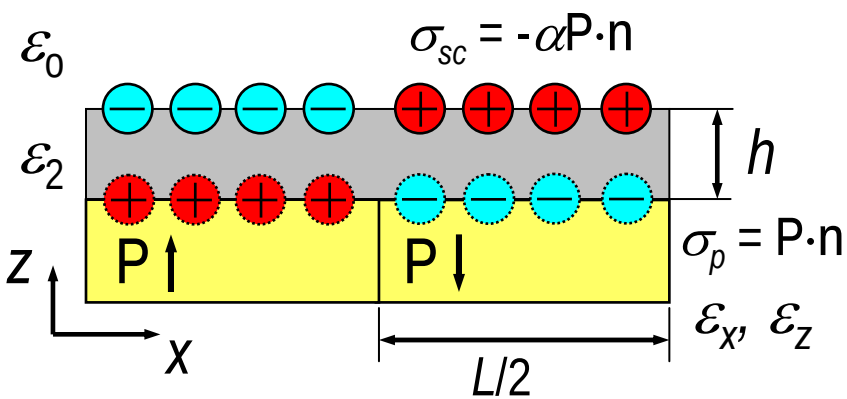

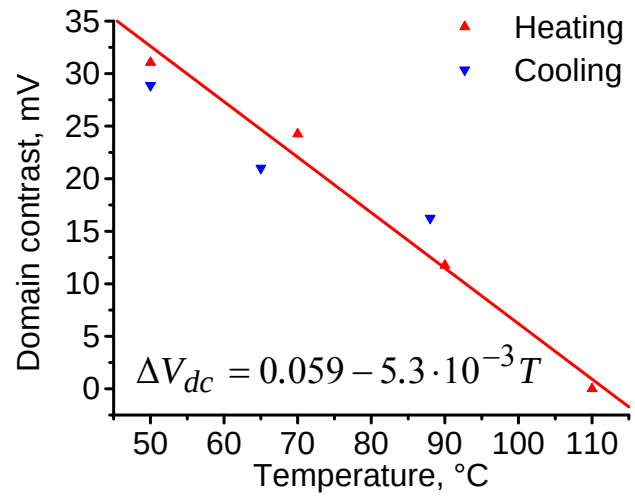

Domain potential contrast vs. T

Equilibrium degree of screening:

$$\alpha = T\frac{P}{qN_a}\frac{\Delta S_{ads}}{a_1} - \frac{P}{qN_a}\frac{\Delta H_{ads}}{a_1} - \frac{a_2}{a_1}$$

SSPM contrast vs. degree of screening

$$\Delta V_{dc} = \alpha\frac{2h\sqrt{\varepsilon_x\varepsilon_z}P}{\varepsilon_2\left(\varepsilon_0 + \sqrt{\varepsilon_x\varepsilon_z}\right)} - \beta H(1-\alpha)\frac{P}{\varepsilon_0 + \sqrt{\varepsilon_x\varepsilon_z}}\ln\left(\frac{H}{4d}\right)^{-1}$$

Experimental results:

ΔH_{ads} = 164.6 kJ/mole

ΔS_{ads} = -126.6 J/mole K

E_a = 4 kJ/mole

τ = ~15 min

SSPM on Ferroelectric Surface

1. Polarization charge is completely screened on $BaTiO_3$ (100) surface; variation of temperature in formation of uncompensated charge.
2. Dynamics of phase transition and numeric value of potential suggest that screening is due to surface adsorbates.
3. Kinetics and thermodynamics of adsorption can be determined from VT SSPM measurements.

NanoTransport System

PLD growth and in-situ Characterization of Surface and Transport Properties of Oxide Films

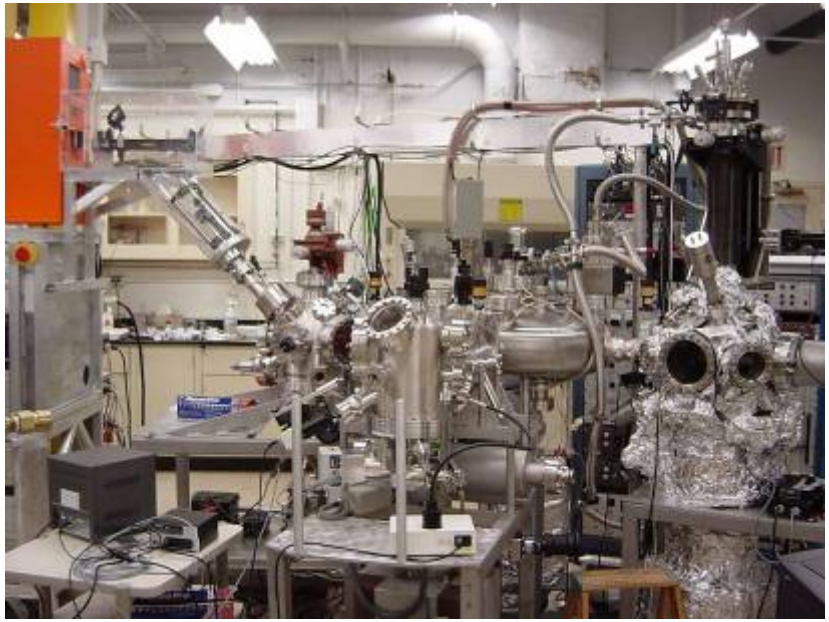

Art Baddorf

Sergei Kalinin

Junsoo Shin

Combination of in-situ synthesis, surface science characterization and UHV scanning probe microscopy for oxide surface films

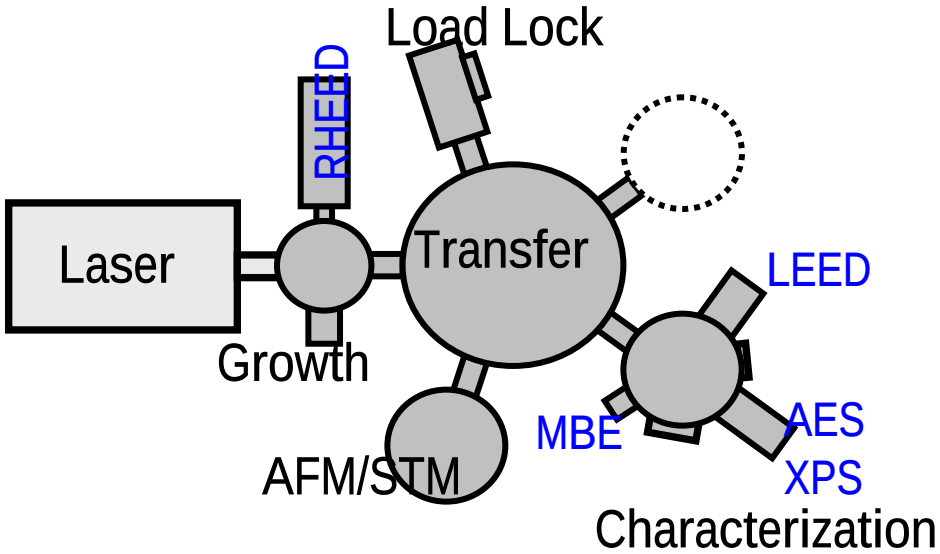

E.W. Plummer (UT)

Surface stability of epitaxial $SrRuO_3$ films ($SrRuO_3/SrTiO_3$)

Contamination by air exposure

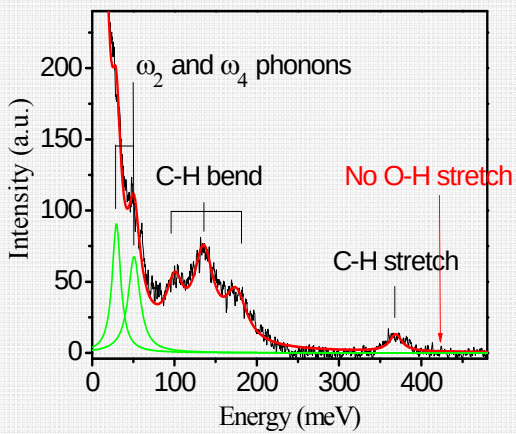

HREELS spectrum

Low density hydrocarbon contamination (< 1 ML)

X-ray Photoelectron Spectroscopy

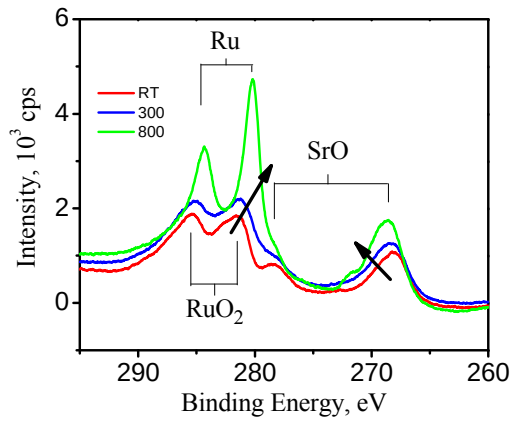

- Ru peaks : BE decreases by annealing → reduced oxide, $Ru^{4+}_{SrRuO3} \Rightarrow Ru^0 + O_2(g)$
- Sr peaks: BE increases by annealing → SrO is chemically stable, $Sr^{2+}_{SrRuO3} \Rightarrow Sr^{2+}_{Sr\ rich\ phase}$.

Thermal Desorption Spectroscopy

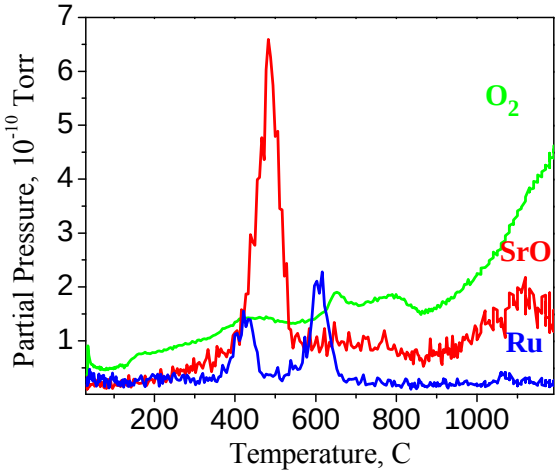

- Desorption of SrO and Ru is observed in two regimes: (400~600°C) and (> 900°C)
- No peaks for Sr metal or ruthenium oxides

Surface stability of epitaxial $SrRuO_3$ films ($SrRuO_3/SrTiO_3$)

Decomposition Pathway of air-exposed $SrRuO_3$ Films

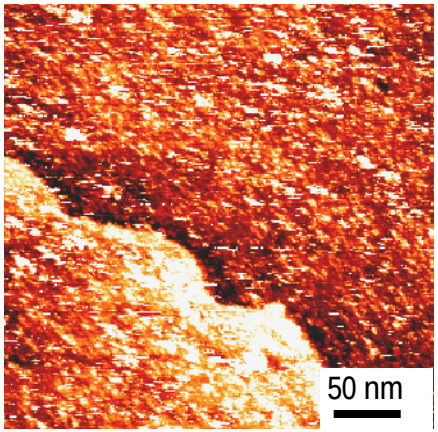

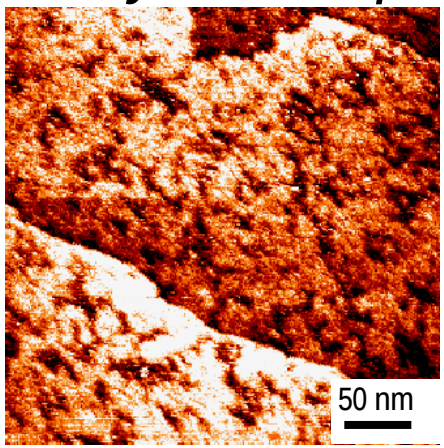

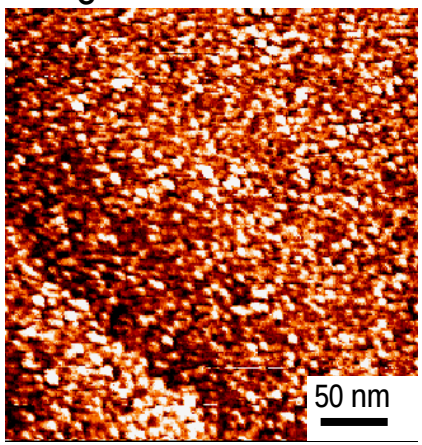

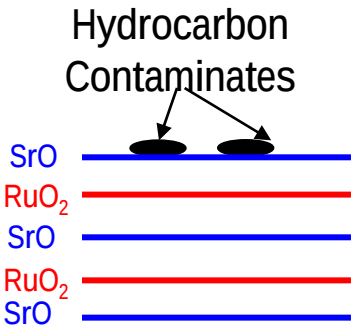

RT ~ 100ºC

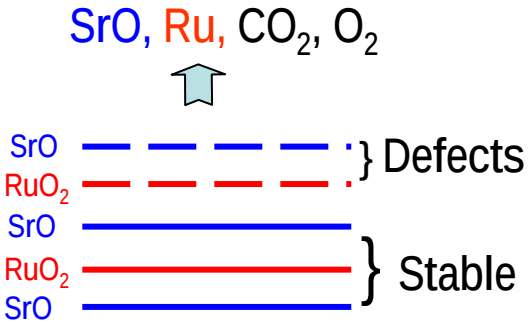

300ºC ~ 500ºC

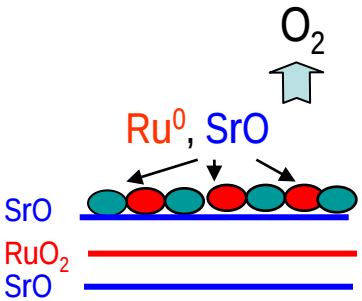

600ºC ~ 800ºC

- RT ~ 100°C : atomic step, hydrocarbon contamination (HREELS)
- 300 ~ 500°C : observed holes due to desorption of SrO, Ru, CO_2, O_2 (TDS, XPS)
- 600 ~ 800°C : formation and growth of metallic Ru^0, SrO nanoparticles. (XPS)

Atomic resolution STM of $SrRuO_3/SrTiO_3$

- Ideal electrode material for oxide based devices
- Interface structure: atomic resolution of electrode $SrRuO_3$ (defects and atomic structure)

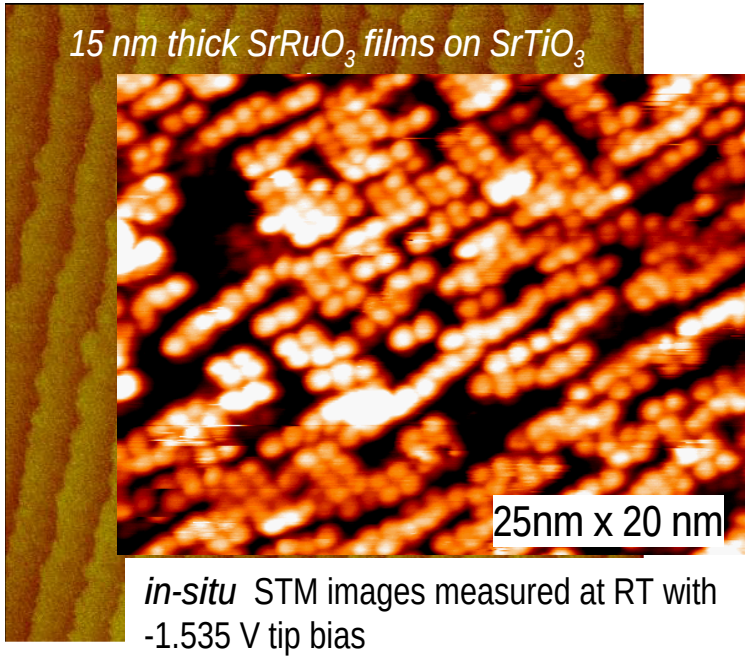

in-situ STM images measured at RT with -1.535 V tip bias

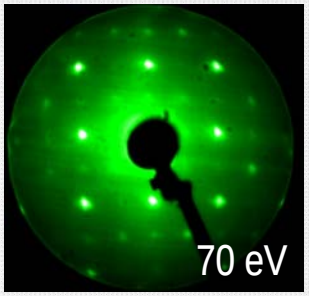

p(2x2) in-situ LEED

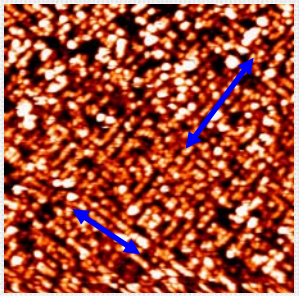

in-situ STM (50 nm^2)

Several possible crystal domain orientations of orthorhombic $SrRuO_3$ on cubic $SrTiO_3$ coexist in one thin films.

- Large atomic defect density (only observed in STM image)
- Short range ordered atomic rows
- Surface reconstruction reminiscent of orthorhombic structure

Growth of $BaTiO_3$ films on $SrRuO_3/SrTiO_3$ by PLD

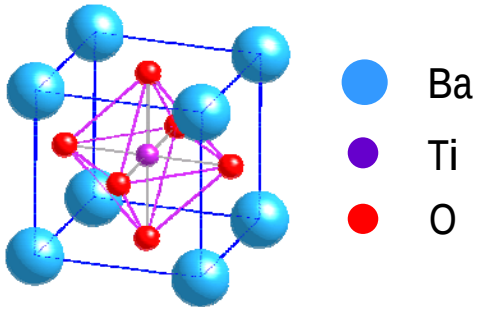

2.23 % in-plane lattice mismatch (RT)

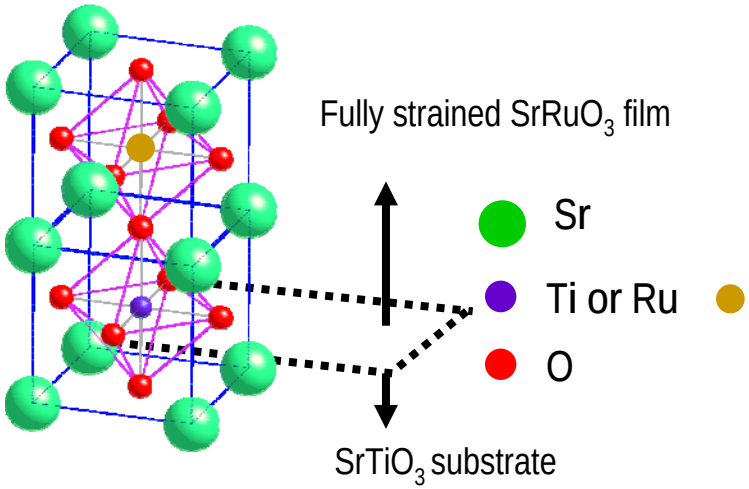

Expected termination $BaTiO_3$ films: BaO
Termination $SrRuO_3$ electrode: SrO
Termination $SrTiO_3$ substrate: TiO_2

RHEED oscillation and pattern
(layer by layer growth)

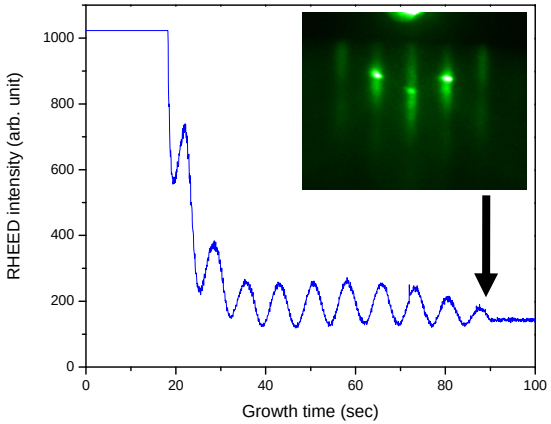

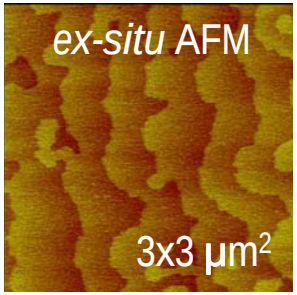

10 ML $BaTiO_3$ films on $SrRuO_3/SrTiO_3$

RHEED oscillation and pattern
(layer by layer growth → step flow growth)

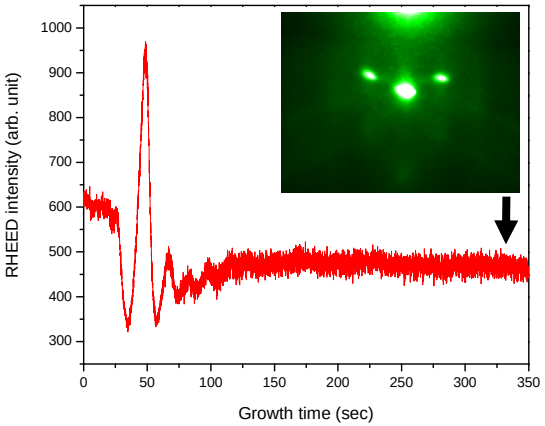

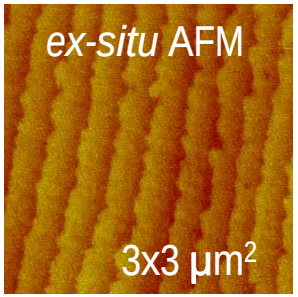

15 nm thick $SrRuO_3$ films on $SrTiO_3$

Evolution of LEED patterns with $BaTiO_3$ film thickness

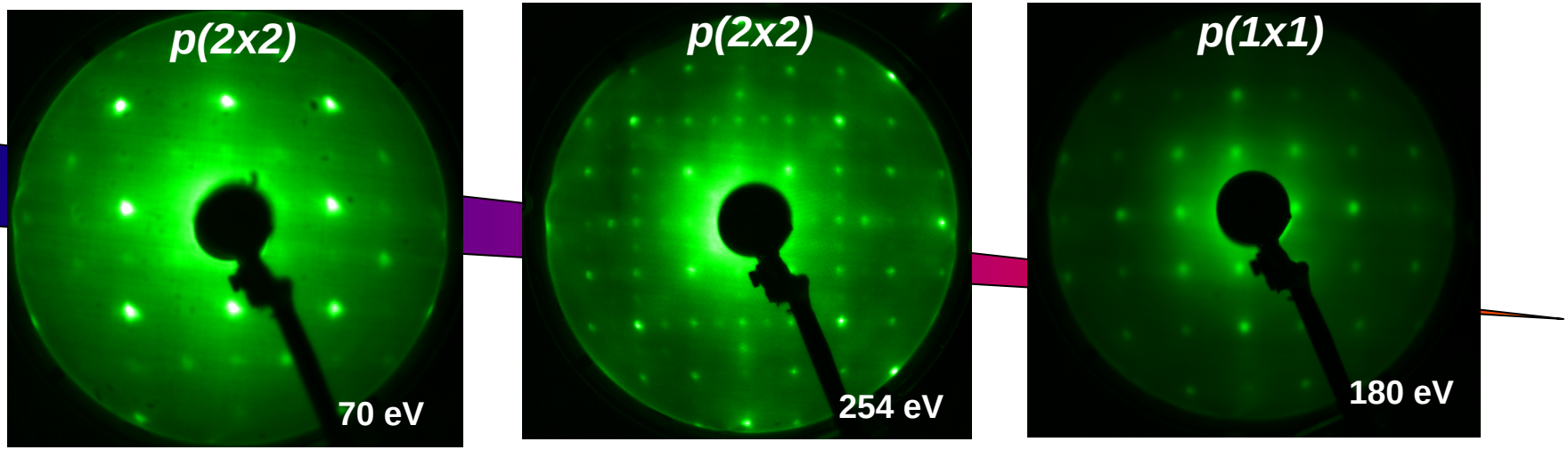

Pristine $SrRuO_3/SrTiO_3$

1~2 ML $BaTiO_3$ on $SrRuO_3/SrTiO_3$

4 ML $BaTiO_3$ on $SrRuO_3/SrTiO_3$

Several possibilities for p(2x2) reconstruction in 1~2 ML thick films

- The diffraction of the buried $SrRuO_3$ structure is observed through the thin $BaTiO_3$ films.
- Due to the mixed layer at the interface with both Sr and Ba oxide.
- The p(2x2) reconstruction of the $SrRuO_3$ effects the $BaTiO_3$.

  Possibly induced octahedral tilting in $BaTiO_3$ films. → metallic properties in $BaTiO_3$ films???

Surface polar structure of $BaTiO_3$ exposed to H_2O

LEED patterns for 10 ML $BaTiO_3$ films

Clean surface

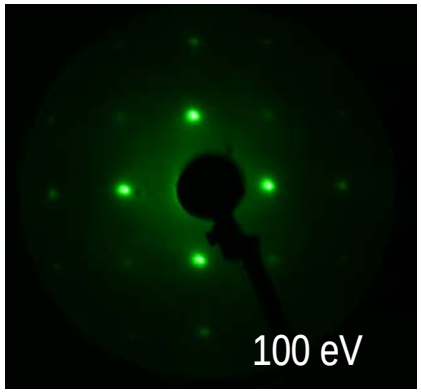

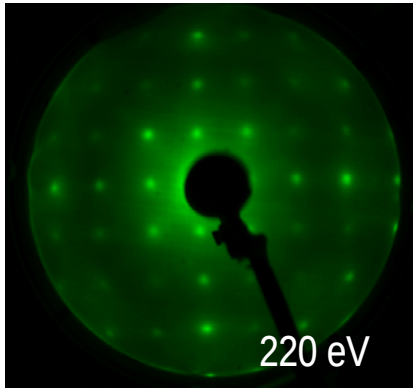

Exposure to H_2O for 10 min ($P_{H2O} = 10^{-4}$ Torr)

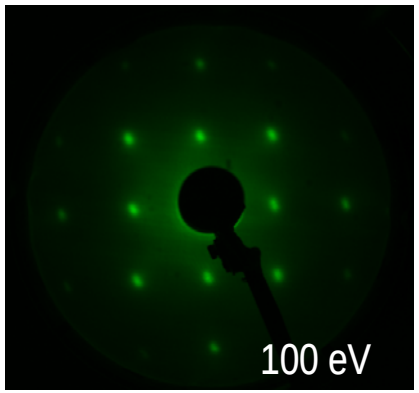

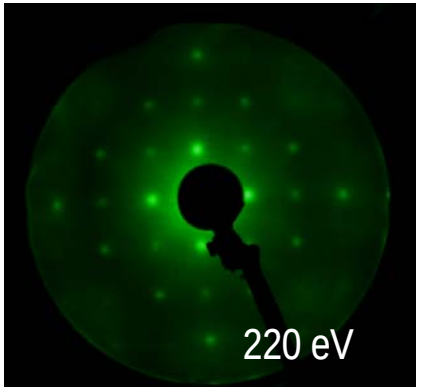

Exposure to H_2O for 1 hour ($P_{H2O} = 10^{-4}$ Torr)

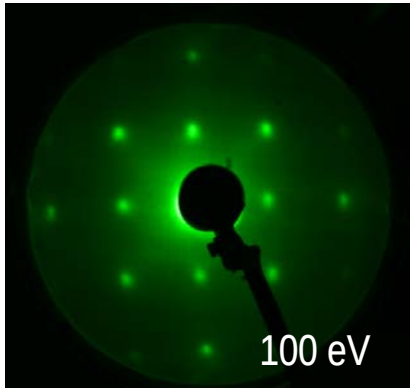

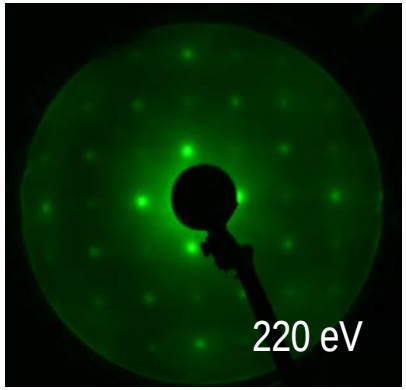

All cases: (1 x 1) LEED pattern observed.

Summary of R_p factors and polarizations

	R_p factor	Polarization
Clean 10 ML (RT)	0.32	Up
Clean 4 ML (RT)	0.30	Up
Clean 4 ML (LT)	0.45	Up (???)
Clean 1~2 ML (RT)	0.52	???
10 ML exposed to H_2O (RT)	0.39	Down (?)

Films are polar. Is polarization switchable?

First results: PFM of $BiFeO_3$ films in UHV

Out-of-plane PFM

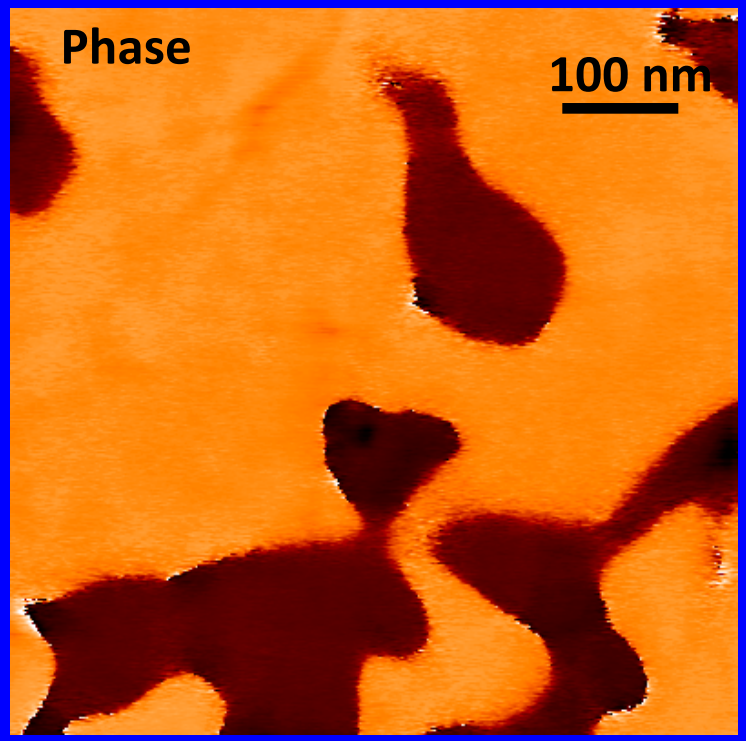

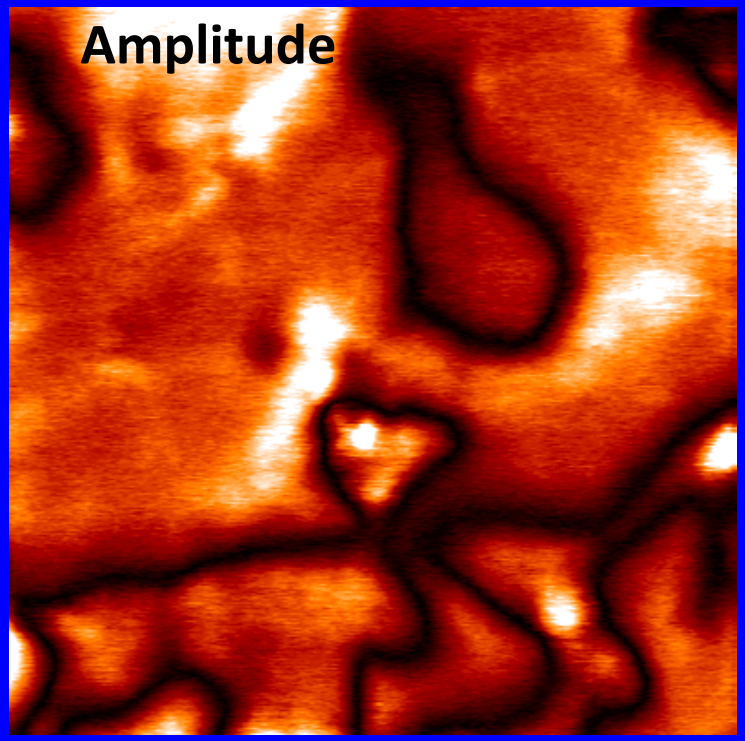

Operating frequency: 5 kHz to 1 MHz – resonantly enhanced PFM (contact ω_0 > 100 kHz)

Switching Spectroscopy and Band Excitation PFM (Q-measurement) successfully implemented.

Note: For 2 and 5 nm films monodomain out-of-plane polarization turns into polydomain state upon annealing at ~ 250 C in p = 10^{-3} of O_2.